SLAC–PUB–95–6801
September 1995

Heavy Beam Loading in Storage Ring Radio Frequency Systems*

M. G. Minty** and R. H. Siemann***

Stanford Linear Accelerator Center,

Stanford University, Stanford, CA 94309

Abstract

Effects arising from both steady-state and transient beam loading of an rf system in circular accelerators are described. The stability of the rf system and the particle beam is studied using a numerical model of the beam-cavity interaction with multiple feedback loops. Nonlinearities in the power source are also considered. As a special case, a detailed model of the Stanford Linear Collider damping rings is presented. The effects of beam-induced transients and intensity jitter on the rf system are analyzed and are used to determine stability tolerances for incoming current variations. A low current limit is demonstrated and techniques are described to ease this limit. Implications for the design and operation of future storage ring rf systems are studied in the heavily beam-loaded limit.

Submitted to *Nuclear Instruments and Methods*

---

*Work supported by Department of Energy contract DE–AC03–76SF00515.
**e-mail minty@slac.stanford.edu
***e-mail siemann@slac.stanford.edu

1. Introduction

The rf systems of many synchrotrons, storage rings, and damping rings are heavily beam loaded. Transient loading of the rf system can result in a time-dependent bunch length and time-dependent phase at extraction or at the interaction point. Beam loading is usually analyzed making simplifying assumptions. These may include neglecting nonlinearities, assuming idealized elements—such as rf power sources that do not limit, ignoring coupling between feedback loops, or not considering abnormal operating conditions—such as an improperly injected pulse. Our experience with heavy beam loading in the Stanford Linear Collider (SLC) damping rings seemed to indicate that the beam and/or rf system can become unstable well below the current expected based on the steady-state analysis of the system.

The generic circuit model for the beam-loaded rf system is given in Fig. 1. For a relativistic bunched beam, the voltage induced by the beam is negligible compared to the beam energy; therefore, the beam is represented as a current source. This current $\vec{I}_b$, which is at angular frequency ω_{rf}, is equal to twice the dc beam current. We assume that there is an isolator between the rf power source and the cavity, so that the power source can also be represented as a current source [1]. The sum of the generator and beam currents is the total cavity current $\vec{I}_c = \vec{I}_g + \vec{I}_b$, which drives the cavity at angular frequency ω_{rf}. The cavity is modeled as a resonant circuit with an impedance large only in the immediate vicinity of the frequency of the resonator. The cavity has quality factor Q, angular resonant frequency ω_0, shunt impedance R, and impedance Z. The impedance may be described [2] by a parallel RLC circuit. The total cavity voltage is $\vec{V}_c = \vec{I}_c Z$. The tuning angle,

$$\phi_z = \tan^{-1}\left[2Q\,\frac{(\omega_0 - \omega_{\mathrm{rf}})}{\omega_0}\right] , \tag{1}$$

is the angle between $\vec{I_c}$ and $\vec{V_c}$. Expressed in terms of ϕ_z, the impedance is

$$Z(\phi_z) = \frac{R}{1 - j\tan\phi_z} , \tag{2}$$

with $j = \sqrt{-1}$. The cavity is inductive with V_c leading I_c for $\phi_z > 0$, or is capacitive with V_c lagging I_c for $\phi_z < 0$.

The beam-induced voltage is retarding at short times after a single passage of the beam through the cavity. For the sign convention of Fig. 1, the beam current used in the equivalent circuit $\vec{I_b}$ is therefore 180° out of phase with the actual beam current $\tilde{\mathrm{I}}_b$. The phasor diagram corresponding to the circuit model of Fig. 1 is shown in Fig. 2 at a fixed time, and for a capacitive cavity and a beam above transition. The dashed line shows the direction of the actual beam current, which lags behind the cavity voltage. The phase of the beam ϕ_b is measured with respect to the crest of the rf. In terms of the energy loss per turn due to synchrotron radiation (U_0) and higher order modes (U_{hom}), the equilibrium value of ϕ_b is the synchronous phase $\phi_s = \cos^{-1}[(U_0 + U_{\mathrm{hom}})/V_c]$. The angle between the generator current and cavity voltage is the loading angle, ϕ_l. With no beam, the loading angle is equal to the tuning angle. The projection of the total current onto the cavity voltage is the shunt resistor current, $I_0 = V_c/R$.

In this paper, we analyze the effects of heavy beam loading on rf systems. Examples are given for the SLC damping rings, for which parameters are given in Table I. First, the dynamics of steady-state beam loading are reviewed; then, a numerical model for an rf system with feedback loops is described in detail. Simulations with the model are then used to characterize the transient response of the system. Tolerances for dynamic stability of the beam and rf system are analyzed and used to study techniques which may relax limitations arising from transient beam loading.

II. Steady-state beam loading

K. Robinson derived two high-current limits in 1964 [3]. The first of these leads to the requirement for a negative tuning angle, $\phi_z < 0$, above transition. The second pertains to the restoring force seen by the beam. The total cavity voltage $\vec{V_c}$ is the phasor sum of the beam induced voltage $\vec{V_b}$ and the voltage produced by the rf generator $\vec{V_g}$. The restoring force depends on the slope of $\vec{V_g}$ alone since the beam-induced voltage is always at the same phase with respect to the beam current [4]. That is, only the generator contributes to phase stability.

The relationship between the various voltages and phase angles is sketched in Fig. 3 at the limit of the high-current instability for which the actual beam current is in phase with the generator voltage. Shown in Fig. 3a is the phasor diagram, while the projections onto the real axis as a function of time is given in Fig. 3b. Applying the law of sines to the phasor diagram gives $V_c/\sin|\phi_z| = V_b/\sin\phi_b$. Since ϕ_z is negative for a capacitive cavity, $V_c \sin\phi_b = -V_b \sin\phi_z$ at the limit. With $V_b = I_b R \cos\phi_z$, the high-current limit is

$$V_c > -\frac{I_b R}{2} \frac{\sin 2\phi_z}{\sin\phi_b} . \tag{3}$$

Introducing the beam loading ratio $Y = I_b/I_0$ and including the upper limit from the usual Robinson's instability,

$$-\frac{2}{Y} \sin\phi_b < \sin 2\phi_z < 0 . \tag{4}$$

These conditions constrain the tuning angle and, for a fixed cavity voltage, also constrain the beam current.

A. *Direct feedback*

Direct feedback is described in Ref. [5]. In the equivalent circuit, shown in Fig. 4, a fraction of the cavity voltage $\beta\vec{V}_c$ is phase shifted and subtracted from the drive signal to the klystron. The loop gain is $H = \beta SZ \exp\left[j(\phi_e + \omega\tau_t)\right]$, in which S is the transconductance of the klystron, τ_t is the total time delay around the loop, and ϕ_e is an externally supplied phase shift. To ensure negative feedback, this angle is nominally adjusted to compensate for the time delay when the cavity is tuned to resonance; i.e., $\phi_e + \omega_{\rm rf}\tau_t = 0$. From the circuit model, the effect of the feedback is equivalent to that of a new circuit with no feedback with a new shunt resistor current $I_0{}^* = (1 + H)I_0$. The effective cavity resistance is $R^* = R/(1 + H)$ and since R/Q is determined by the cavity geometry, the Q is lowered by $(1 + H)$. The feedback therefore raises the instability threshold by $1 + H$. The effective tuning angle $\phi_z{}'$ is the angle between the new generator current which includes the feedback current and the total cavity voltage. The relationship to the tuning angle without direct feedback ϕ_z is given by $\tan\phi_z' = \left[(1/(1 + H))\tan\phi_z\right]$.

B. *Implementation at the SLC*

Difficulties related to heavy beam loading in the SLC damping rings were first encountered while operating with an rf voltage ramp, where the amplitude of the rf wave was decreased to intentionally lengthen the bunch [6]. Using the parameters for the SLC damping rings, and using Eq. (3), a voltage limit of about 400 kV is obtained at $I_b = 160$ mA and $\phi_z = -45°$. Below this voltage, the beam was observed to be unstable. To overcome this difficulty, direct feedback was added, and the cavity voltage could be further reduced. However, unexplainable difficulties were encountered while operating with higher current beams. Before describing the numerical model that was developed in part to address these questions, we examine how the maximum output power of the klystron may limit operation at high beam currents.

C. Power limitations

A relationship between the beam current $\vec{I}_b$, generator power P_g, and cavity voltage $\vec{V}_c$ can be derived using the equations developed in Ref. [1]. The result is

$$I_b = \frac{V_c}{R\cos\phi_z}\left[\pm\sqrt{\cos^2(\phi_z-\phi_b)+\left[\frac{8R\beta_c P_g}{V_c^2(1+\beta_c)}\right]\cos^2\phi_z - 1} - \cos(\phi_z-\phi_b)\right], \tag{5}$$

where β_c is the cavity coupling coefficient. This expression remains valid in the presence of feedback loops. Using the parameters of the SLC, Eq. (5) is plotted for $V_c = 1$ MV in Fig. 5 for different generator powers. Along the line of zero loading angle, the power reflected from the cavity is minimized. With a 60 kW power limit, the steady-state upper limit on the beam current is about 350 mA at $\phi_l = 0$. The power limit is far less than the Robinson stability limit, which is shaded in the figure. With less available klystron power, the limit on the total beam current is correspondingly reduced. To relax this limit, the total cavity voltage may be lowered. Plotted in Fig. 6 is $I_b(\phi_z)$ at five different cavity voltages. At low cavity voltage, the beam loading stability criterion is more restrictive because the generator current is reduced. The power limit meanwhile is less restrictive because there is sufficient power to compensate for the beam-induced voltage.

Figures 5 and 6 suggest that klystron characteristics and transient beam loading may affect system stability. First, the contour of maximum klystron power determines the maximum operable, steady-state beam current for a given cavity voltage. At high currents which require more than the available power, the cavity voltage would not be maintained. Secondly, referring to Fig. 5 if the tuning angle is less than -40°, more than 60 kW would be required from the klystron in the event of a low current or missing pulse. As will be shown, the response of the klystron (for example, if it saturates) can have negative consequences for the feedback loops and for recovery of subsequent pulses.

III. The radio frequency system model

A block diagram of the beam-loaded rf system with feedback is shown in Fig. 7. There are two additional loops: the amplitude feedback loop of gain G_a, which is used to maintain the desired cavity voltage V_{des}, and the phase feedback loop of gain G_p, which regulates the phase of the beam relative to an external phase ϕ_{des}.

A. *Beam-cavity interaction*

The equation of motion for the beam phase using the sign convention of Fig. 1 is

$$\frac{d^2\phi_b}{dt^2} = -\frac{\alpha\omega_{\text{rf}}}{E_0 T_0}\left[V_c \cos(\phi_b - \phi_c) + (U_0 + U_{\text{hom}})\right] , \tag{6}$$

where α is the momentum compaction factor, E_0 is the beam energy, T_0 is the revolution period, and ϕ_c is the angle between the total cavity voltage and an external phase reference. While the beam is stored, the beam current is assumed to be time-independent; i.e.,

$$|I_b| \;=\; \text{constant} \;. \tag{7}$$

This is valid for the case of the SLC damping rings for which the impedance of the accelerating cavities is narrow compared to the frequency spectrum of the beam. Equations 6 and 7 are the equations for the beam.

Kirchhoff's laws give the equation of motion for the total cavity voltage:

$$\frac{d^2\vec{V_c}}{dt^2} + \frac{\omega_0}{Q}\frac{d\vec{V_c}}{dt} + {\omega_0}^2\vec{V_c} = \frac{R\omega_0}{Q}\frac{d\vec{I_c}}{dt}. \tag{8}$$

For a fixed frequency rf system, the equations for the cavity voltage and total current may be transformed to the reference frame which rotates at the frequency of the generator. This reduces the cpu time required in a simulation by a factor approximately equal to $\omega_{\mathrm{rf}}/\omega_s$, where ω_s is the angular synchrotron frequency. In the case of the SLC this ratio is about 7000. The transformation is

$$\vec{V_c}(t) = \left[V_{c_r}(t) + jV_{c_i}(t)\right] e^{j\omega_{\mathrm{rf}}t}, \tag{9}$$

and similarly for the total cavity current. Here the subscripts r and i denote the real and imaginary parts of the relevant variable. In the limit of a slowly varying voltage amplitude, $dV_c/dt << V_c\omega_{\mathrm{rf}}$, two coupled, first-order differential equations result:

$$2Q\,\frac{dV_{c_r}}{dt} + \frac{dV_{c_i}}{dt} + \omega_{\mathrm{rf}}V_{c_r} + 2Q\,(\omega_0 - \omega_{\mathrm{rf}})V_{c_i} \;=\; R\omega_{\mathrm{rf}}I_{c_r} \tag{10}$$

and

$$2Q\,\frac{dV_{c_i}}{dt} - \frac{dV_{c_r}}{dt} + \omega_{\mathrm{rf}}V_{c_i} - 2Q\,(\omega_0 - \omega_{\mathrm{rf}})V_{c_r} \;=\; R\omega_{\mathrm{rf}}I_{c_i}\;. \tag{11}$$

These equations give the time evolution of the cavity voltage.

B. *Klystron*

A block diagram for the klystron is shown in Fig. 8a. The klystron has an input impedance R_{in}. The coupling β_c of the cavity to the waveguide is represented by an ideal transformer. An isolator between the klystron and cavity absorbs any power reflected from the cavity due to cavity detuning. There are four sources of phase shift across the klystron. The group delay in the klystron and the time delay in the waveguides are modeled in the frequency domain using a third order Pade approximation [7] for $\exp\{-j\omega\tau_k\}$, where τ_k is the total delay. The frequency response of the klystron is modeled using a Butterworth filter, which produces a flat response in the passband $0 < \omega < \omega_c$, where ω_c is the angular cutoff frequency. The amplitude response for an nth order filter is given by

$$\frac{V_{\text{out}}}{V_{\text{in}}}(\omega) = \frac{1}{\sqrt{1+(\frac{\omega}{\omega_c})^{2n}}} \tag{12}$$

Note that a passband filter, when transformed to the reference frame that rotates at the angular rf frequency, is equivalent to a low pass filter with the same bandwidth and rolloff characteristics. In the model, the combined time delay of the klystron and waveguides is 120 ns. The measured klystron 3 dB bandwidth is 1/2 (5.6) MHz and rolls off at 60 dB per decade. Finally, there is a phase shift that depends on the klystron input power. The nonlinear, power-dependent phase shift is modeled using an interpolation table from measured data.

Referring to Fig. 8b, the input power is $P_{\text{in}} = {V_{\text{in}}}^2/2R_{\text{in}}$, where V_{in} is the input voltage. The output power P_g includes the transmitted cavity power and the reflected power absorbed by the isolator. Satisfying the boundary conditions between the waveguide and cavity, the power to the load P_l is

$$P_l = \left[1-\left(\frac{\beta_c-1}{\beta_c+1}\right)^2\right] P_g = \frac{4\beta_c}{(1+\beta_c)^2}\, P_g\ . \tag{13}$$

The circuit model for the amplitude response of the klystron is shown in Fig. 8b. The transconductance S converts voltage to current. The cavity coupling has been transformed to the cavity side of the transformer. The power to the load is $P_l = I_l V_l/2$, where the factor 2 converts from rms to peak voltage, by definition $I_l = SV_{\text{in}}$, and $V_l = SV_{\text{in}}\left[R/(1+\beta_c)\right]$. These expressions give

$$P_l = \frac{R}{2(1+\beta_c)}\,(SV_{\text{in}})^2 \quad \text{or} \quad S^2 = \frac{1+\beta_c}{R_{\text{in}}R}\left(\frac{P_l}{P_{\text{in}}}\right) . \tag{14}$$

Using Eq. (13) for P_l,

$$S = \sqrt{\frac{4\beta_c}{(1+\beta_c)R_{\text{in}}R}\left(\frac{P_g}{P_{\text{in}}}\right)} . \tag{15}$$

This equation is used to represent the klystron.

The saturation curve for the SLC klystron is plotted in Fig. 9a. The points indicate measured data scaled from 50 to 60 kW maximum output power. The klystron saturates at 60 kW at an input power of about 0.5 W. Shown in Fig. 9b is the power curve for a limiter which is included just upstream of the klystron. Beyond an input power of 1.4 W, the limiter output is extrapolated to a hard limit. The limiter is tunable and nominally adjusted to rolloff just below klystron saturation. The calculated saturation characteristics of the klystron and limiter combined are shown in Fig. 9c.

C. Feedback loops

Feedback loops are used to stabilize the beam and the accelerator. In longitudinal phase space, these generally include voltage and phase feedback. Typically, the accelerating voltage is regulated to compensate for unwanted changes, which may include deviations arising from thermal effects or from slow changes in the beam-induced voltage with beam current. Phase loops are often used to ensure proper injection and extraction, or to minimize the amplitude of synchrotron oscillations. The cavity voltage and beam phase feedback loops are usually designed to be independent of one another. However, direct feedback, which compensates for heavy beam loading, acts on the vector rf voltage so that both voltage and phase are controlled. The following contains descriptions of the feedback loops at the SLC, and describes how these loops are modeled in our simulation program.

i. AMPLITUDE FEEDBACK LOOP

The amplitude feedback loop maintains the cavity voltage at some desired level V_{des}. At the SLC, this loop regulates the amplitude sum of the cavity voltages. A block diagram for the loop is shown in Fig. 10a. In the SLC there are 2 cavities each containing 2 cells. The cell voltages are detected with pickup loops and converted to dc with peak detectors. An error signal V_δ is generated and amplified with a variable gain amplifier that has a bandwidth equal to the product of the fixed capacitance and the variable resistance. An additional difference amplifier may be used to make fast changes to the cavity voltage by an amount V_m. The output of this amplifier controls an rf attenuator of gain A through a linearization circuit. The rf signal is amplified and directed towards the klystron. If the direct feedback loop gain is nonzero (see below), then a switch is used to provide amplification of this signal by an amount that depends on the gain of the direct loop, H.

The circuit model for this loop is shown in Fig. 10b. The voltages V_1 and V_2 represent the amplitude of the voltages on the two rf cavities. The variable gain amplifier in Fig. 10a is represented in the model as a constant gain bandwidth amplifier whose gain and bandwidth characteristics are determined by g_{a_1} and g_{a_2}. An interpolation table is used to model the measured insertion loss of the rf attenuator with its linearization circuit. The amplitude of the output rf, AV_{in}, is nominally proportional to the linearization circuit input, or control voltage V_{con}. In practice, however, the combined effect of the linearization circuit and rf attenuator can be nonlinear. Shown in Fig. 11a is the measured insertion loss $A(V_{\mathrm{con}})$. Because the slope $\mathrm{d}A/\mathrm{d}V_{\mathrm{con}}$ is not constant, the small signal gain of the loop changes depending on V_{con}. These data are used in the interpolation table. The measured small signal gain in the feedback path as a function of V_{con} is shown from two separate measurements in Fig. 11b. Note that the gain is proportional to the output voltage of the master oscillator.

ii. PHASE FEEDBACK LOOP

The phase feedback loop, shown in Fig. 12a, regulates the phase of the beam with respect to an external rf source. At the SLC, this source is the linear accelerator (linac); a phase error of zero corresponds to extracting the beam at the correct phase for good capture into the linac. The relative phase of the beam ϕ_b in the ring is detected using an electrode of a beam position monitor. The component at 4 ω_{rf}, which is the linac frequency, is obtained using a bandpass filter. The phase error is formed by mixing this signal with the linac rf, which is shifted in phase by the phase reference ϕ_{des}. The signal is then filtered and amplified. The resulting signal is used to adjust the phase of the damping ring rf, using an rf phase shifter.

Figure 12b is the circuit model of the loop. When the equations of motion have been mixed to baseband, mixing corresponds to taking a difference of phases. Here, the phases are referenced to the ring rf frequency, and are the same as when referenced to linac rf frequency. The phase of the beam is compared with the desired phase ϕ_{des} and the difference is filtered and amplified. The amplifier is a constant gain-bandwidth amplifier with the gain of the loop given by

$$\frac{V_{\text{out}}}{V_{\text{in}}}(\omega) = \frac{g_{p_1}}{1+g_{p_1}g_{p_2}}\left[\frac{1}{1+j\,\dfrac{\omega}{\omega_c\left(1+g_{p_1}g_{p_2}\right)}}\right], \tag{16}$$

where g_{p1} is the amplifier open loop gain, $g_{p_1}g_{p_2}$ is the loop gain, ω_c is the cutoff frequency, and the 3 dB bandwidth is $\omega_c(1+g_{p_1}g_{p_2})$. The difference between this signal and the phase of the drive signal ϕ_{IN} is the phase of the rf into the klystron.

iii. DIRECT FEEDBACK LOOP

The direct feedback loop [5,8] is shown in Fig. 13a. The rf voltage from each cell is detected, attenuated, phase shifted as appropriate, and combined with 3 dB hybrids to give the phasor sum. The phasor sum of the two cavities is similarly obtained. The summed signal is then phase shifted by an amount ϕ_e, which is adjusted experimentally to ensure that the loop remains stable. This signal is then amplified and summed with the drive signal. The circuit model for the loop is shown in Fig. 13b. After combining cavity voltages to obtain the total voltage, the signal is phase shifted, amplified, and delayed. The amplifier gain β represents the combined gain of the cavity pickup and electronic amplification. A 240 ns time delay for signal propagation is included, and is modeled using a Pade approximation. When this loop is closed, to compensate for cavity detuning, the gain of the amplitude feedback loop is increased by $(1 + H)$ because that gain is proportional to the master oscillator voltage.

D. Numerical model

The circuit representation for the numerical model of the SLC damping ring rf system is shown in Fig. 14. There are two accelerating cavities and a single klystron. The feedback loops (from Figs. 10, 12, and 13) and klystron (Fig. 8) contain filters, denoted by rectangles, with the indicated 3 dB bandwidths and rolloffs. The equations of motion for the beam-cavity interaction [Eqs. (6), (7), (10), and (11)] are also programmed. The external inputs required for integration are shown. These include the beam current $\tilde{I}_b$, the desired cavity voltage V_{des}, two tuning angles ϕ_{z_1} and ϕ_{z_2}, the voltage and phase from the rf source V_{IN} and ϕ_{IN}, the external phase required for stability of the direct feedback loop ϕ_e, and (when implemented) the desired voltage for fast changes to the cavity voltage V_m. The phase from the master oscillator ϕ_{IN} is shifted by ϕ_{inj} which is adjusted to ensure proper capture of the beam at injection.

The equations are integrated using Matrix$_x$ by Integrated Systems [9]. This software product was designed for analyzing circuit equations and is used at the SLC in the design of the feedback loops for the beam trajectories. For linear systems, Matrix$_x$ allows for feedback design using state-space formalisms. For our nonlinear system, we use the integration routines in Matrix$_x$ along with the user-friendly graphics interface. The beam dynamics are naturally described by an equation for the beam phase ϕ_b, while the equations for the cavity are in terms of the real and imaginary parts of the total voltage, $\tilde{V}_{c_r}$ and $\tilde{V}_{c_i}$. The relationship between these equations is found by transforming between rectangular and polar coordinates.

In all applications, the initial conditions for the steady-state response are determined and then loaded back into the program. Then one or more of the inputs is perturbed and the effect on the system output is viewed. The motivation for beginning with the steady-state response is based on both physical and practical arguments. Under nominal operating conditions, the rf system is already in a stable configuration and processes like extraction of the beam are perturbations to the system. Specifically, we are interested in the dynamics of the beam-loaded rf system relative to the steady-state solution with beam. For programming, the total cpu time required for finding the equilibrium point is considerably less than that required for doing a time domain simulation to achieve the same result.

An example of a simulation result compared with an SLC experiment is shown in Fig. 15. Here, properties of the direct feedback loop were examined. In the experiment, for each value of loop gain H, the phase in the direct feedback ϕ_e was changed to determine its range of stability. The gain of the loop is limited by the total time delay around the loop, which has contributions from the klystron, the waveguides, and the delay in the feedback path, which includes the external phase shift ϕ_e. In the simulation, the effect of the slow cavity-tuner feedback loops was modeled by adjusting the cavity loading angle to zero for each value of loop gain. The inputs to the simulation are the cavity voltage, the beam current, the loop gain, and the variable phase ϕ_e. Plotted in Fig. 15 is the phase range for stable operation $\delta\phi_e$, as a function of H. The calculated stable phase range is in good agreement with the measured range. The maximum attainable loop gain corresponds to a phase range of zero. In both the measurement and the simulation, the maximum loop gain is near 19 dB under these conditions.

IV. Transient beam loading

The effects of beam-induced transients and intensity jitter on the rf system are analyzed and used to determine stability tolerances for high-current and low-current pulses. As will be shown, amplitude regulation of normal events and stability against missing pulses depend critically on the maximum available klystron power. In the SLC, missing pulses are common, with a frequency of several per hour, due to pulsed element failures and/or interlocks at the injector gun. Transient beam loading can cause the klystron to saturate. As a consequence, the rf system may not regulate, and then both the bunch length and beam phase at extraction may become time dependent.

A. Beam-induced transients

When a particle beam is injected into or extracted from a circular accelerator, beam-induced electromagnetic fields cause the accelerating cavity voltage to oscillate at the synchrotron frequency. For fast cycling storage rings, the magnitude of the oscillations depends on the time between extraction and injection of beam pulses, the cavity fill time, and on the beam current. While advantageous for increasing the steady-state high current limit, direct feedback is also useful in reducing the magnitude of these oscillations.

Transients in the SLC damping rings induced by extraction and injection of beam are shown in Fig. 16, with direct feedback ($H = 6$, solid curve) and without ($H = 0$, dotted curve). The extracted and injected beams are of equal intensity. The rf phase $\phi_{\rm IN}$ is shifted by $\phi_{\rm inj}$ to minimize the amplitude of the transient oscillation at injection. The loading angle, which is zero in the steady state, becomes nonzero when the beam is extracted, and then returns to zero after the beam is injected and the transients have damped. Whereas the total power required is the same in the steady state with and without direct feedback, the instantaneous power requirement is much higher with direct feedback. Because the cavity fill time is reduced by $1 + H$ with direct feedback, the cavity, and therefore also the klystron, respond quickly to the voltage and phase errors resulting from the absence of beam. Without direct feedback, the cavity voltage is regulated by the amplitude feedback, which responds relatively slowly. The oscillations in the cavity voltage at the synchrotron frequency are therefore not corrected. With the direct feedback properly tuned, residual oscillations in the cavity voltage and beam phase still persist; the voltage and phase errors introduced by extracting the beam are improperly compensated for at injection because the klystron has saturated. Further reduction of the transient oscillations is discussed in Section V.

The peak-to-peak variations in the voltage δV_c are shown in Fig. 17a while those of the beam phase $\delta\phi_b$ are shown in Fig. 17b as a function of the direct feedback loop gain H. With $H = 0$, $\delta V_c/V_c \approx 50\%$, while $\delta\phi_b \approx 65°$. With $H > 3$, $\delta V_c/V_c \approx 20\%$, while $\delta\phi_b \approx 20°$. Without direct feedback, the size of the residual oscillations depends on the time between extraction and injection of the beam. Conceivably, this time could be adjusted to cause the transient at extraction to interfere destructively with the injection transient. However this time is not typically a free parameter. With direct feedback, the size of the residual oscillations is independent of this time (provided that regulation is maintained), and depends only on the available klystron power.

With a nonlinear klystron, beam-induced transients can result in an improperly regulated cavity voltage. This is shown graphically in Fig. 18, where V_c, P_g, and ϕ_l are plotted as a function of time at six different beam currents. The tuning angle is adjusted at each current to maintain $\phi_l = 0$ in the steady state with beam. At low beam currents the perturbations due to extraction and injection are relatively small; only modest power is required from the klystron. The gain of both the amplitude and direct feedback loops is proportional to the small signal gain of the klystron, which depends on $\mathrm{dP_g/dP_{in}}$ evaluated at $\mathrm{P_{in}}$. At low currents, the small signal gain is large, since the klystron is operated far from saturation. As the beam current is increased, more power is required in the steady state, and the small signal gain approaches zero. Just below saturation, any change in the klystron input power produces little effect on the output power. At $I_b = 200$ mA, the small signal gain is zero during the time in which the klystron has saturated. At $I_b = 250$ mA, the effect of the transients is to cause the klystron to operate beyond saturation between the time of extraction at 10 μs and about 50 μs. Under these conditions, the small signal gain is of opposite sign so that the amplitude feedback and direct feedback loops supply positive instead of negative feedback. In this case, extraction and injection transients combine in a way which leads to recovery of positive small signal gain, even though the klystron was operating over the knee in the saturation curve. At 300 mA beam current, the klystron is unable to recover and the cavity voltage is not maintained.

Regulation of the cavity voltage is examined in more detail in Fig. 19 for the last two cases of Fig. 18. With marginal recovery at 250 mA, the feedback loops behave as expected when the small signal gain is positive. At 300 mA, however, the amplitude loop integrates the voltage error that results from klystron saturation. In response, the requested klystron input power grows monitonically, thereby causing the klystron to operate even further from the initial steady-state operating point. In practice, the maximum klystron input power is usually limited with an rf limiter, or by low-level amplifiers upstream of the klystron (in Fig. 14, the limit would be set by the 53 dB of low-level amplification). Whether or not the system can resume regulation depends on the properties of the limiter and low-level amplifiers.

B. Intensity jitter

Variations in the intensity of the incoming beam are considered tolerable for the rf system if the cavity voltage is regulated to the desired value. For a fast cycling storage ring with a store time much smaller than the bandwidth of the tuner feedback loops, the effect of injecting a pulse of different current is a change in the steady-state loading angle ϕ_l. This in turn requires more klystron power. As discussed previously, the rf system is stable, provided that the combined effects of the transients induced by extraction and injection of the beam are such that the klystron returns to a state of positive small signal gain. The response of the rf system to intensity fluctuations is shown in Fig. 20 for two different nominal beam currents. In this example, the intensity fluctuations are much larger than typical variations in the beam current. The horizontal time axis is arbitrary provided that the store time is short compared to the response time of the cavity tuner feedback loops, and long enough for the transients to have damped. The damping time for the transients is determined by Robinson damping [1] and is longer for lower currents. In the low-current case, the cavity voltage always returns to the desired value. In the high-current case, the cavity voltage is not maintained and the rf system is unstable. The inability to regulate is clearly evidenced in the error signal in the amplitude feedback loop.

C. *Stability tolerances*

Generally, with a realistic nonlinear klystron and a power limiter, the highest beam currents are obtainable for $\phi_l = 0$. In practice, however, with a power-limited klystron, the tightest constraint on the maximum operable beam current arises from missing or low-current pulses. At very high currents, and with a high direct feedback loop gain, the time during which the beam is absent between fills or gaps between bunch trains may limit the maximum beam current.. Plotted in Fig. 21 is the percentage tolerable current jitter $|\delta I_b/I_b|$ as a function of I_b along the line $\phi_l = 0$. Changes in the beam intensity are considered tolerable provided the rf system is able to regulate the cavity voltage in the steady state. In these simulations, the steady-state beam current I_b is extracted, and a new pulse of current $I_b + \delta I_b$ with $\delta I_b > 0$ is injected. The rf system is easily able to regulate with large increases in the beam current, except at the highest currents. With $I_b = 0.20$ A, for example, the rf system would remain stable if a subsequent pulse of 40% above nominal, or 0.28 A, were injected into the ring. The solid vertical line indicates a hard limit due to a missing pulse. With $I_b = I_m$, the klystron is driven by the direct feedback loop towards saturation when the beam is absent. A subsequent pulse would experience an arbitrary cavity voltage. The time required for the system to become stable depends on the response time of the slow tuner feedback loops and on the output of low-level amplifiers, which may limit the maximum klystron input power. This hard limit presents the strictest limit on the maximum current. At the SLC, with a cavity voltage of 1 MV, a 60 kW klystron output power, and the cavity tuned to $\phi_l = 0$, stability against missing pulses is ensured only for $I_b < I_m$ with $I_m = 0.1725$ A. To accommodate 0.22 A current in the most recent run, the cavity voltage was reduced, thereby requiring less klystron power.

D. Parameter space for voltage regulation

In previous examples, the loading angle ϕ_l has been constrained to be zero, as is nominally maintained by slow tuner-feedback loops. Generally, this condition need not be satisfied, provided that there is additional power available and that power reflected from the cavities is absorbed in an isolator between the cavities and klystron. As will be shown, under conditions of heavy beam loading, intentional detuning ($\phi_l \neq 0$) is advantageous for two reasons. First, it provides stability against beam-induced transients by exploiting the nonlinearity of the klystron. Second, cavity detuning may be used to relax stability tolerances for low current or missing pulses.

Plotted in Fig. 22 are V_c, P_g, and ϕ_l as a function of beam current for a tuning angle fixed at -45°. In these simulations, the extracted and injected beams have equal intensity. At low currents, the cavity is grossly mismatched ($\phi_l < 0$) in the steady state. As the current is increased, the steady-state value of ϕ_l passes through zero and becomes more positive. Notice that the peak-to-peak amplitude of the voltage oscillations is largest for $\phi_l = 0$. This is due to the large difference in the klystron output power in the steady state and in saturation. Cavity detuning can therefore be used to minimize the transients at injection. In addition, notice that the steady-state power required is large for both low and high beam currents as a result of cavity detuning. In this example, the small signal gain is close to zero for both $I_b < 35$ mA and $I_b > 270$ mA. Perturbations caused by injection and extraction of beam may therefore cause the klystron to saturate: not only high-current beams, but also low-current beams can result in loss of regulation of the cavity voltage.

The parameter space for voltage regulation in the steady state is shown in Fig. 23. The beam current is plotted as a function of tuning angle.

The solid curve with no symbols is the analytic calculation, Eq. (5), for a 60 kW klystron. Along $\phi_l = 0$, the maximum current is 360 mA, with a hard limiting klystron. The current limit is reduced to 240 mA due to transient beam loading with the nonlinear klystron (curve with closed circles). With the power limiter (curve with open circles), the current limit is increased to 290 mA. With a perfectly linear klystron, the cavity voltage would be regulated to 1 MV for operation anywhere within the area bounded by the analytic curve and the horizontal and vertical axes. In order to operate outside this region, either the klystron power would have to be increased or the cavity voltage lowered.

The simulations include the dynamics of the beam-cavity interaction in the presence of multiple feedback loops and the nonlinear klystron. From Fig. 9, the nonlinearity of the klystron can result in reducing, or even changing, the sign of the small signal gain of the amplitude and direct rf feedback loops. Avoiding the latter is critical to prevent a runaway unstable situation. This can be accomplished with proper limiting of the klystron input power.

V. Implications for storage ring radio frequency system design and operation

Analysis of the available operating space for voltage regulation (Fig. 23) and tolerances to current jitter (Fig. 21) may be used to make an estimate of the required klystron output power. At high beam current and high cavity voltage, however, the required power may be unrealistic. In this section, methods will be described to optimize the stability of the rf system at high currents, while minimizing the power requirements of the klystron.

Plotted in Fig. 24 is the parameter space for voltage regulation for a 1 MV cavity voltage subdivided into three characteristic regions. The solid curve bounding Regions 1–3 is Eq. (5) for a 60 kW klystron. The curve with circles is the result with the nonlinear klystron with the power limiter. Region 3 is unstable against perturbations to the system. The vertical line separating Regions 1 and 2 represents the limit associated with missing pulses (see Fig. 21). Consider any beam current along the line $\phi_z = \phi_{z,m}$; for example, $I_b = I_m$ or $I_b = I_{c'}$. When this pulse is extracted, the loading angle becomes large and negative as the slow tuner feedback loops have insufficient bandwidth to track the change; the operating point moves downwards (toward $I_b = 0$) on this vertical line. A voltage error related to the change in the beam-induced voltage is detected by the feedback loops that regulate the cavity voltage. If direct feedback is used or if the cavity and amplitude loop bandwidth are fast relative to the time during which the beam is absent, then the klystron is driven to larger output power in an attempt to compensate for this error. Because the gain of the amplitude feedback loops depends on the local slope of the klystron saturation curve, as the feedback drives the klystron harder, the gain of the loop simultaneously decreases,

The required klystron output power may be estimated from the missing pulse limit. For a properly matched cavity ($\phi_l = 0$) and known operating voltage, the klystron should deliver as much power as required to avoid saturation due to a missing pulse. Rewriting Eq. (5),

$$P_g = \frac{V_c^2(1+\beta_c)}{8R\,\beta_c\cos^2\phi_z}\left[\left(\frac{I_bR}{V_c}\right)^2\cos^2\phi_z + \frac{2I_bR}{V_c}\cos\phi_z\cos(\phi_z-\phi_b)+1\right], \tag{17}$$

which gives the required generator power in terms of the beam current I_b, the cavity voltage V_c, and the cavity tuning angle ϕ_z. Expressed in terms of the loading angle ϕ_l, the tuning angle is calculable from the phasor diagram of Fig. 2. Since

$$I_0 + I_b \cos\phi_b = I_g \cos\phi_l , \tag{18}$$

$$I_0 \tan\phi_z + I_b \sin\phi_b = I_g \sin\phi_l , \tag{19}$$

and $I_0 = \frac{V_c}{R}$, then

$$\tan\phi_z = \left(1 + \frac{I_b R}{V_c}\cos\phi_b\right)\tan\phi_l - \frac{I_b R}{V_c}\sin\phi_b . \tag{20}$$

The tuning angle at $\phi_l = 0$ and I_m is

$$\phi_{z,m} = -\tan^{-1}\left(\frac{I_m R}{V_c}\sin\phi_b\right) . \tag{21}$$

Substituting $\phi_{z,m}$ into (17) gives the klystron power required to be stable against missing pulses when the nominal beam current is I_m:

$$P_{g,m}|_{\phi_l=0} = \frac{V_c^2(1+\beta_c)}{8R\beta_c}\left[1 + \left(\frac{I_m}{I_0}\right)^2 \sin^2\phi_b\right] . \tag{22}$$

Notice that the steady-state power is less than that required for a missing pulse. For example, with $I_b = I_m = 0.17A$, $V_c = 1$ MV, and $\phi_b = 80°$, then $\phi_{z,m} = -40°$. To remain stable against missing pulses, the maximum klystron output is $P_{g,m}|_{\phi_{z,m}=-40°} = 59.5$ kW, while the steady-state power output during operation at $I_m = 0.17$ A is $P_g|_{\phi_{z,m}=-40°} = 46.1$ kW.

A. Extension of the missing pulse limit by cavity detuning

By detuning the cavity such that $\phi_l > 0$, more beam current can be stored stably for the same maximum klystron power. By changing the setpoints for the tuner feedback loops to detune the cavity, stability against missing pulses can be obtained for the same maximum power klystron, but at higher current. From Eq. (5), the maximum current I_c operable while maintaining stability against missing pulses results when the two terms in the square brackets are equal; i.e.,

$$I_c = -\frac{2V_c}{R\cos\phi_z}\cos(\phi_z - \phi_b) \ . \tag{23}$$

For the above example, $I_c = 0.26$ A. The loading angle $\phi_l|_{I_b=I_c}$ is obtained from Eq. (20).

The required total klystron output power as a function of desired beam current is plotted in Fig. 25. To maintain regulation while operating along $\phi_l = 0$, the required power is $P_{g,m}$ evaluated at $I_b = I_m$. From the previous example, with $I_m = 0.17A$ along $\phi_l = 0$, 60 kW maximum klystron output power was required. With cavity detuning the required power is $P_{g,m}$ evaluated at $I_b = I_c$; for the same maximum, klystron output power stability is maintained for currents up to $I_c = 0.26$ A with the loading angle tuned to 20°. Under these conditions, $P_{g,m}$ and the steady-state power output are equal. Notice that Eq. (22) underestimates slightly the required power in the detuned limit. The nonlinearity of the klystron produces a difference in the analytic estimate (I_c) and simulation ($I_c{}'$) at high beam currents (see Fig. 24).

B. *Optimal use of klystron power by radio frequency system conditioning*

To achieve higher beam currents for the same maximum klystron output power, the klystron must be made to operate more efficiently. For operation in Region 2 of Fig. 24, the hard limit due to missing pulses or absence of beam must be overcome. This may be accomplished by adjusting the reference to the direct feedback loop. Highlighted in Fig. 26 are the voltage error ΔV and the phase error $\Delta\phi$ that result from an absent beam. During the time the beam is absent, the direct feedback compensates for these errors and drives the klystron into saturation. Ideally, the rf system might be conditioned by adjusting $\vec{V}_g$ without beam to $\vec{V}_c$ with beam during the time when $I_b = 0$. Because the klystron is power limited, however, this is impossible. Alternatively, the input to the direct feedback loop can be adjusted in the event of a missing or low-current pulse to avoid saturating the klystron and to eliminate regulation problems on subsequent pulses.

i. THE RADIO FREQUENCY SYSTEM CONDITIONING

By conditioning the amplitude of the input voltage to the direct feedback loop, regulation of the cavity voltage is ensured in the event of a missing or low-current pulse. Residual oscillations from improper phase compensation may be corrected by conditioning the phase of the rf input to the direct feedback loop. A block diagram for rf system conditioning is shown in Fig. 27. In the most simple implementation, a beam presence signal enables a voltage correction (ΔV) and a phase correction ($\Delta\phi$) in the event of a missing pulse. Along $\phi_l = 0$, the reference voltage required to correct the amplitude variation of the cavity is

$$V_{\text{des}|I_b=0} = V_{g|I_b\neq 0} = -V_b \, \frac{\sin(\phi_b - \phi_z)}{\sin\phi_z} \; . \tag{24}$$

The change in the reference phase ϕ_{des} required to correct the phase variation of the cavity is

$$\Delta\phi = \phi_z - \phi_l \; . \tag{25}$$

A switch disables the correction ($\Delta V_{\text{des}} = 0$ and $\Delta\phi_{\text{des}} = 0$) in anticipation of the next pulse. More generally, the voltage and phase correction could depend on the input current. The rf system conditioning is thereby applied to low current, as well as missing pulses. In practice, the amount by which to lower the voltage reference V_{des} is to that value for which the control voltage V_{con} from the amplitude feedback loop is unchanged by the change in beam current at injection. The amount by which to change the phase reference ϕ_{des} is that which will minimize the change in the cavity voltage phase angle.

Simulation results using rf conditioning for the case of a missing pulse are shown in Fig. 28. In this example, the beam current is well above the missing pulse limit (see Fig. 21). Without rf conditioning, the klystron operates well beyond the knee of the saturation curve during the time in which the beam is absent. When the beam is injected, the amplitude and direct feedback loops supply positive instead of negative feedback. The cavity voltage is not regulated, and it responds directly to the beam-induced transients and the cavity voltage. With conditioning of the voltage alone, the voltage reference is reduced when the missing pulse is detected. The next pulse is anticipated and the reference is raised. During the time in which the beam was absent, the klystron is brought out of saturation by lowering the reference voltage. The cavity voltage is well regulated and the change in the control voltage V_{con} at injection is minimized. With conditioning of the phase, in addition to conditioning the voltage, the transients in the beam phase and cavity voltage are further reduced.

Figure 29 shows the peak-to-peak voltage and phase oscillations with rf system conditioning, and a direct feedback loop gain $H = 6$ as a function of the time at which the voltage and phase reset or correction is applied. In these simulations, the magnitude of the voltage and phase offsets have been optimized for injection at $\delta t = 0$. Without direct feedback, the peak-to-peak cavity voltage variation δV_c was 500 kV, or $\delta V_c/V_c = 50\%$ (see Fig. 17). With $H = 6$, $\delta V_c/V_c$ was reduced to 20%. With both $H = 6$ and rf conditioning, $\delta V_c/V_c = 7\%$. For the beam phase, $\delta\phi_b$ is reduced from 70° to 20° by using direct feedback. With the direct feedback and rf system conditioning $\delta\phi_b = 6°$.

ii. STABILITY TOLERANCES WITH RADIO FREQUENCY SYSTEM CONDITIONING

The rf system conditioning relaxes the tolerance on low-current or missing pulses by adjustment of the reference to the direct feedback loop. Simulations show that all of Region 2 in Fig. 24 is accessible with rf system conditioning of the voltage alone. Figure 30 shows the simulation results at $I_b = 0.29$ A, with $\phi_z = -59°$ and $\phi_l = 0$. This corresponds to $I_b = I_{\max}$ in Fig. 24. The tolerable current jitter is given by Fig. 21, with the missing pulse limit at $I_b = I_m$ eliminated with voltage conditioning. Careful adjustment of the conditioning parameters ΔV and $\Delta\phi$ would allow operation in some parts of Region 3 of Fig. 24; however, because the power output of the klystron is almost equal to its maximum power output, it would be very difficult to further reduce the transients and so avoid crossing the knee of the saturation curve. In practice, therefore, $I_b = I_{\max}$ is the maximum beam current achievable at a given maximum klystron power and cavity voltage.

VI. Conclusion

With conventional feedback systems, including direct feedback, the maximum beam current is limited by the ability of the klystron to maintain constant cavity voltage at high beam current, low current, or in the absence of beam. In the case of the SLC damping rings, performance and the performance limits in Ref. [10] were explained using a detailed model of the rf system. Cavity voltage regulation, and therefore bunch length and beam phase regulation, was shown to be most strongly affected by the largest possible transients arising from either pulse extraction or missing pulses. In the missing pulse limit, rf system and beam instabilities resulted from the interaction of the nonlinear klystron and the feedback loops. A plot of the parameter space for voltage regulation was developed and used to analyze system stability. Cavity detuning was suggested for storing high-current beams in rf systems using conventional feedback with a predetermined maximum klystron output power. Alternatively, the plot may be used to specify klystron performance requirements and feedback loop parameters for future accelerators if the desired particle beam current and nominal rf cavity voltage are known.

The rf system conditioning was developed to allow for most efficient operation of the available klystron power. Due to the effects of transient loading, even with rf system conditioning, the maximum beam current for which the rf system remains stable was shown to be less than estimated by linear analysis. For future storage rings with rf system conditioning, specifications for the required klystron power and feedback loop parameters should involve numerical analysis of the effects of transient beam loading on the rf system. Models for these rings should include more complex situations, including bunch trains and coupled bunch instabilities. We are extending our model to do this.

Acknowledgments

We thank F. Pederson for introducing us to direct feedback at the SLC. We are also grateful to R. Akre, P. Corredoura, G. Dalit, J. Judkins, and H. Schwartz for their contributions and assistance in the measurements. Finally, we thank T. Himel, P. Krejcik, R. Tighe, and P. Wilson for helping us understand the physics and simulation tools.

References

[1] P. B. Wilson, "High Energy Electron Linacs; Application to Storage Ring RF Systems and Linear Colliders," AIP Conf. Proc. No. 87, R. A. Carrigan, F. R. Huson, M. Month, eds., American Institute of Physics, New York (1982); SLAC–PUB–2884 (1982).

[2] G. Dome, "RF Theory," Vol. I, CERN 92–03 (1992).

[3] K.W. Robinson, CEA report CEAL–1010 (1964).

[4] M. Sands, Orsay report 2–76 (1976).

[5] F. Pedersen, IEEE Trans. on Nucl. Sci., NS–22, no. 3 (1975), and NS–32, no. 3 (1985).

[6] P. Krejcik *et al.*, "High Intensity Bunch Length Instabilities in the SLC Damping Rings," Proc. 1993 IEEE Part. Accel. Conf., Washington DC, p. 3240.

[7] L. Kelly, "Handbook of Numerical Methods and Applications," Addison-Wesley Publishing Company, Reading (1967).

[8] P. Krejcik *et al.*, "RF Feedback for Beam Loading Compensation in the SLC Damping Rings," Proc. 1993 IEEE Part. Accel. Conf., Washington, D.C., p. 2370.

[9] Matrix_x by Integrated Systems, Santa Clara, CA 95045.

[10] M.G. Minty *et al.*, "Operating Experiences with High Beam Currents and Transient Beam Loading in the SLC Damping Rings," Proc. 1995 IEEE Part. Accel. Conf., Dallas, Texas.

Table 1: Properties of the beam, cavities, and klystron in the SLC damping rings.

Properties of the beam		Quantity	Unit
E	Energy	1.19	GeV
f_{rev}	Revolution frequency	8.5	MHz
I_b	Beam current (=2× dc current)	variable	A
U_0	Energy loss per turn due to synchrotron radiation	80	keV
k_{hom}	Energy loss factor due to higher order modes	3.2	V/pC
α	Momentum compaction factor	0.015	
Properties of the cavity		**Quantity**	**Unit**
f_{rf}	Accelerating frequency	714	MHz
h	Harmonic number	84	
N_c	Number of rf cavities	2	
N_k	Number of klystrons	1	
R	Loaded shunt impedance per cavity	2.5	MΩ
Q	Loaded quality factor	6860	
V_c	Magnitude of total cavity voltage	variable	V
β_c	Cavity coupling parameter	2.5	
ϕ_z	Cavity tuning angle	variable	degrees
Properties of the klystron		**Quantity**	**Unit**
R_{in}	Klystron input impedance	50	Ω
S_0	Transconductance of linear klystron	0.0552	A/V
τ_k	Klystron and waveguide time delay	120	ns
τ_d	Direct feedback loop delay	240	ns
$P_{g,m}$	maximum klystron output power	60	kW

Figure Captions

1. Circuit model for the generator-cavity and beam-cavity interaction. Both the beam and generator are represented as current sources with currents flowing in the directions indicated.

2. Phasor diagram for a capacitive cavity and a beam above transition with the sign convention for the beam current of Fig. 1. This diagram can be viewed in two coordinate systems. In the first, the phasors rotate counterclockwise and the projections onto the real axis give the time variation. The second system is a coordinate system rotating counterclockwise at the rf frequency. In the steady state, the phasors are stationary in this coordinate system.

3. Phasor diagram for (a) currents and voltages and (b) energy gain as a function of time, both at the stability limit.

4. Circuit model, including direct feedback. The loop gain is H.

5. Dependence of beam current on generator power as a function of tuning angle. The shaded region shows the Robinson stability limit without direct feedback. The dotted line indicates the line of zero loading angle.

6. Dependence of beam current on tuning angle for different cavity voltages. The solid curve corresponds to 60 kW klystron output power. The shaded regions show the Robinson stability limit without direct feedback.

7. Circuit model of a beam-loaded rf system, including amplitude, phase, and direct feedback. The thick solid lines indicate paths for phasors that have both an amplitude and a phase. The thin lines convey either phase or voltage information.

8. (a) Block diagram and (b) circuit model of the amplitude response of the klystron. The (nonlinear) transconductance S of the klystron converts voltage to current.

9. Saturation curve of (a) the SLC klystron and (b) the power limiter. The points are from measurement, while the curves through the data are fits using orthogonal polynomial regression. The straight lines emphasize deviations from linearity. (c) The calculated response of the limiter and klystron combined is also shown.

10. (a) Block diagram and (b) circuit model of the amplitude feedback loop.

11. Measured (a) insertion loss and (b) small signal gain, measured using two different techniques (circles and boxes) as a function of control voltage V_{con} in the amplitude feedback loop path.

12. (a) Block diagram and (b) circuit model of the phase feedback loop.

13. (a) Block diagram and (b) circuit model of the direct feedback loop. The thick lines indicate that both amplitude and phase information are carried.

14. Circuit model of the SLC damping ring rf system. The thick lines indicate paths along which both amplitude and phase information are carried.

15. Stable phase range of the direct feedback loop as a function of loop gain. Measurements in the SLC damping rings are denoted by open circles, while the simulated result is shown using closed circles. The beam current was fixed at $I_b = 0.19$ A. The data were taken with a voltage ramp where the voltage was 950 kV at injection and extraction and 780 kV during the store. These conditions were modeled.

16. Simulations of transient beam loading in the SLC damping ring caused by extraction and injection with and without direct feedback. The cavity voltage V_c, the klystron output power P_g, the loading angle ϕ_l, the beam phase ϕ_b, and the beam current I_b are plotted as a function of time for an direct feedback open loop gain of $H = 0$ (dotted curves) and $H = 6$ (solid curves). The small dots at $I_b = 0$ in the beam phase represent the phase of a single-particle beam.

17. Peak-to-peak variations in (a) cavity voltage δV_c and (b) beam phase oscillations $\delta\phi_b$, as a function of the direct feedback open loop gain.

18. Transient beam loading as a function of beam current I_b with $\phi_l = 0$ in the steady state and varying tuning angle. The cavity voltage V_c, the klystron output power P_g, and the loading angle ϕ_l are plotted as a function of time. At the highest current, the cavity voltage is not maintained due to klystron saturation.

19. Comparison of rf system parameters for $I_b = 250$ mA (marginally stable) and $I_b = 300$ mA (unstable) conditions. The cavity voltage V_c, the klystron input power P_{in}, and the feedback signals of the direct feedback loop V_{rf}, the amplitude feedback loop V_{con}, and the phase feedback loop ϕ_p are plotted as a function of time.

20. Transient beam loading with intensity jitter. The cavity voltage V_c, the klystron output power P_g, the loading angle ϕ_l, the feedback signals of the direct feedback V_{rf} and amplitude feedback V_{con}, and the beam current I_b are plotted as a function of time. At the nominal beam current, $\phi_l = 0$.

21. Tolerable current jitter $\delta I_b/I_b$ as a function of nominal current I_b with $\phi_l = 0$ in the steady state. The solid line at $I_b = I_m = 0.1725$ A represents a hard limit due to a missing pulse.

22. Transient beam loading as a function of beam current I_b with $\phi_z = -45°$ in the steady state and varying loading angle. The cavity voltage V_c, the klystron output power P_g, and the loading angle ϕ_l are plotted as a function of time.

23. Parameter space for voltage regulation. The dependence of the beam current I_b on tuning angle ϕ_z is plotted for a perfectly limiting klystron [solid curve, Eq. (5)], the nonlinear klystron [closed circles, see Fig. 9a], and the nonlinear klystron with the power limiter [open circles, see Fig. 9c]. The dotted curves are contours of constant loading angle ϕ_l.

24. Parameter space for voltage regulation subdivided into three characteristic regions. The vertical line at $\phi_{z,m}$ separates the stable Region 1 from Regions 2 and 3, which may be unstable in the event of a missing pulse. The curve with closed circles includes the nonlinear klystron and power limiter.

25. Analytic estimate of klystron power required in the missing pulse limit with and without cavity detuning at $V_c = 1$ MV.

26. Steady-state cavity voltages. The sum of the generator voltage V_g and beam voltage V_b is the total cavity voltage V_c. When the beam is extracted $V_c = V_g$ and the amplitude and direct feedback loops respond to the voltage error ΔV and the phase error $\Delta\phi$.

27. Block diagram for conditioning of the reference for the direct feedback loop.

28. Cavity regulation with and without conditioning in the event of a missing pulse. Plotted as a function of time are the cavity voltage V_c, the klystron output power P_g, the reference input to the amplitude feedback loop $V_{\rm des}$, the amplitude feedback control voltage $V_{\rm con}$, the reference input to the phase feedback loop $\phi_{\rm des}$, the cavity voltage phase angle ϕ_c, and the beam current I_b. In the first column there is no conditioning. In the second column cavity regulation is established with amplitude conditioning only. In the third column, both amplitude and phase conditioning are applied. The dot-dashed curve in I_b indicates the missing pulse.

29. Peak-to-peak variations in (29a) the cavity voltage δV_c, and (29b) beam phase $\delta\phi_b$ oscillations as a function of the time at which the voltage and phase reset is applied. The direct feedback loop gain is $H = 6$.

30. Cavity regulation with voltage conditioning at $I_b = I_{\rm max}$ in Fig. 24. Plotted as a function of time are the cavity voltage V_c, the klystron output power P_g, the reference input to the amplitude feedback loop $V_{\rm des}$, the amplitude feedback control voltage $V_{\rm con}$, and the beam current I_b. The dotted curve in I_b indicates the missing pulse.

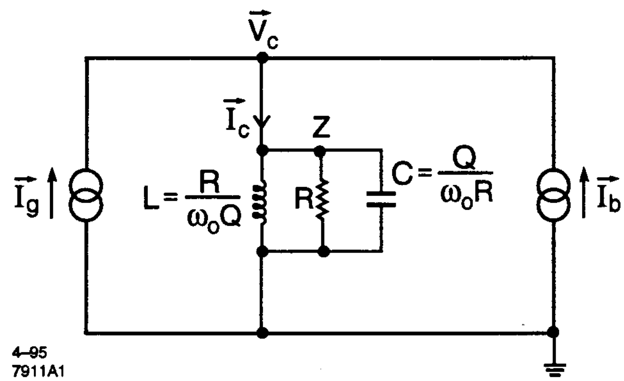

$\vec{V}_c$
$\vec{I}_c$
Z
$\vec{I}_g$
$L = \frac{R}{\omega_o Q}$
R
$C = \frac{Q}{\omega_o R}$
$\vec{I}_b$
4-95
7911A1

Fig. 1

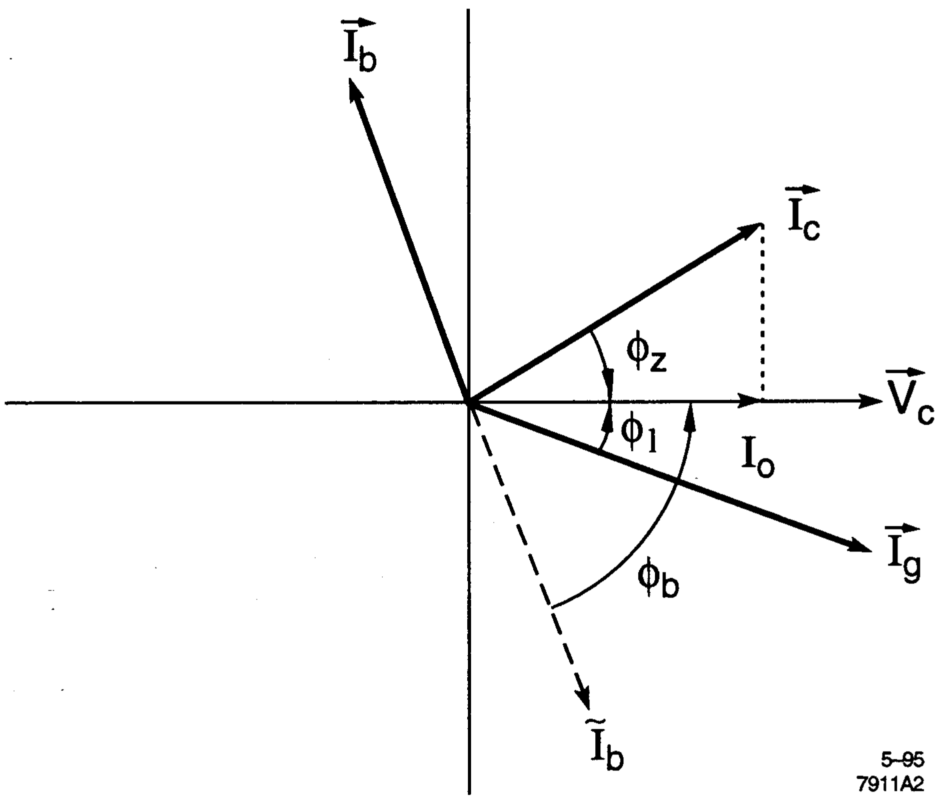

$\vec{I}_b$
$\vec{I}_c$
ϕ_z
$\vec{V}_c$
ϕ_1
I_o
$\vec{I}_g$
ϕ_b
$\tilde{I}_b$
5–95
7911A2

Fig. 2

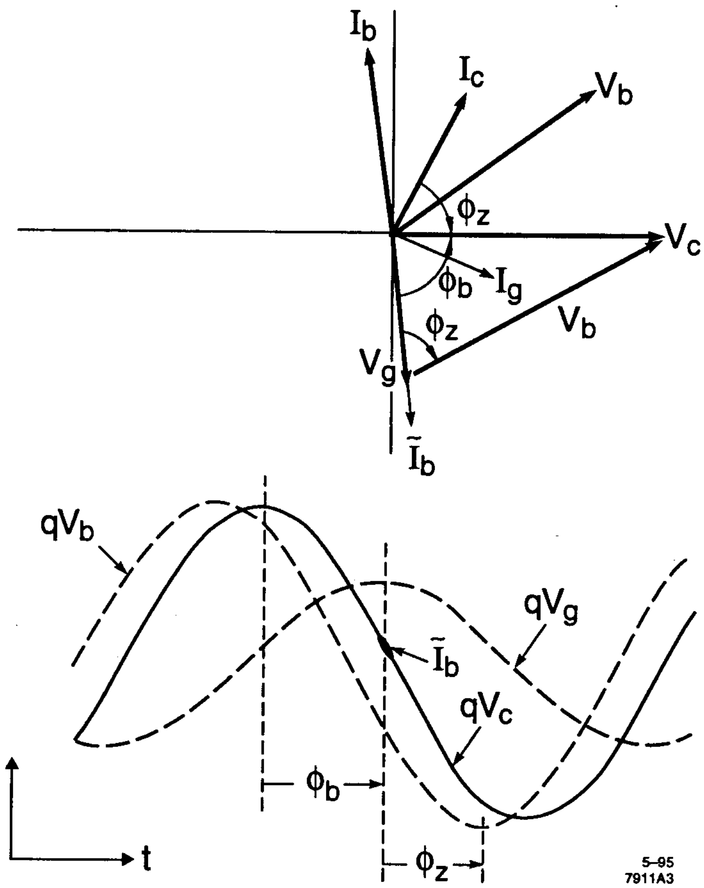

I_b
I_c
V_b
ϕ_z
V_c
ϕ_b
I_g
ϕ_z
V_b
V_g
$\tilde{I}_b$
qV_b
qV_g
$\tilde{I}_b$
qV_c
ϕ_b
t
ϕ_z
5–95
7911A3

Fig. 3

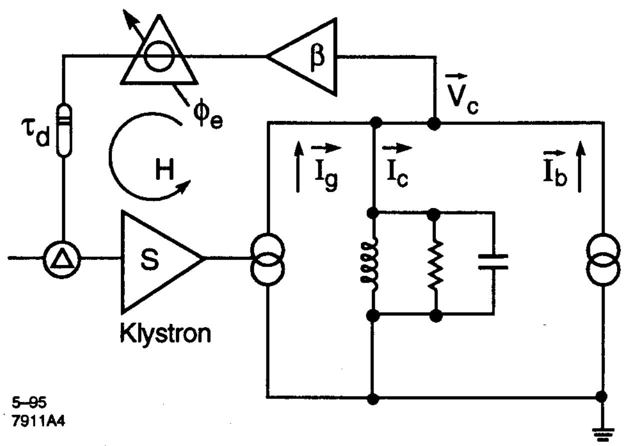

Fig. 4

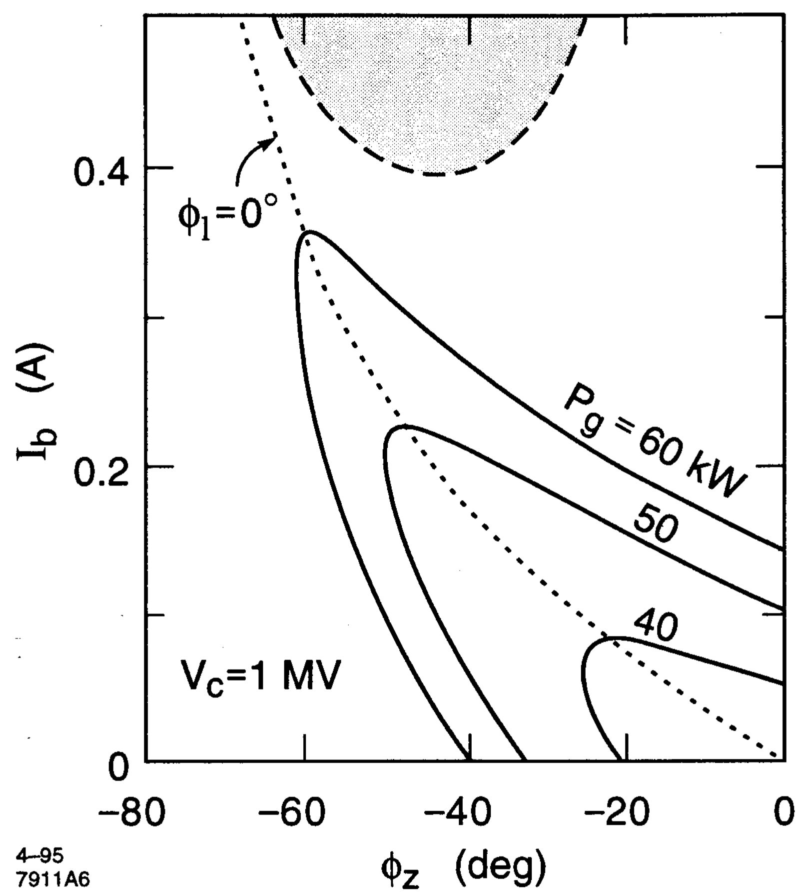
0.4
0.2
0
I_b (A)
$\phi_l = 0°$
$P_g = 60$ kW
50
40
V_c=1 MV
−80
−60
−40
−20
0
ϕ_z (deg)
4–95
7911A6

Fig. 5

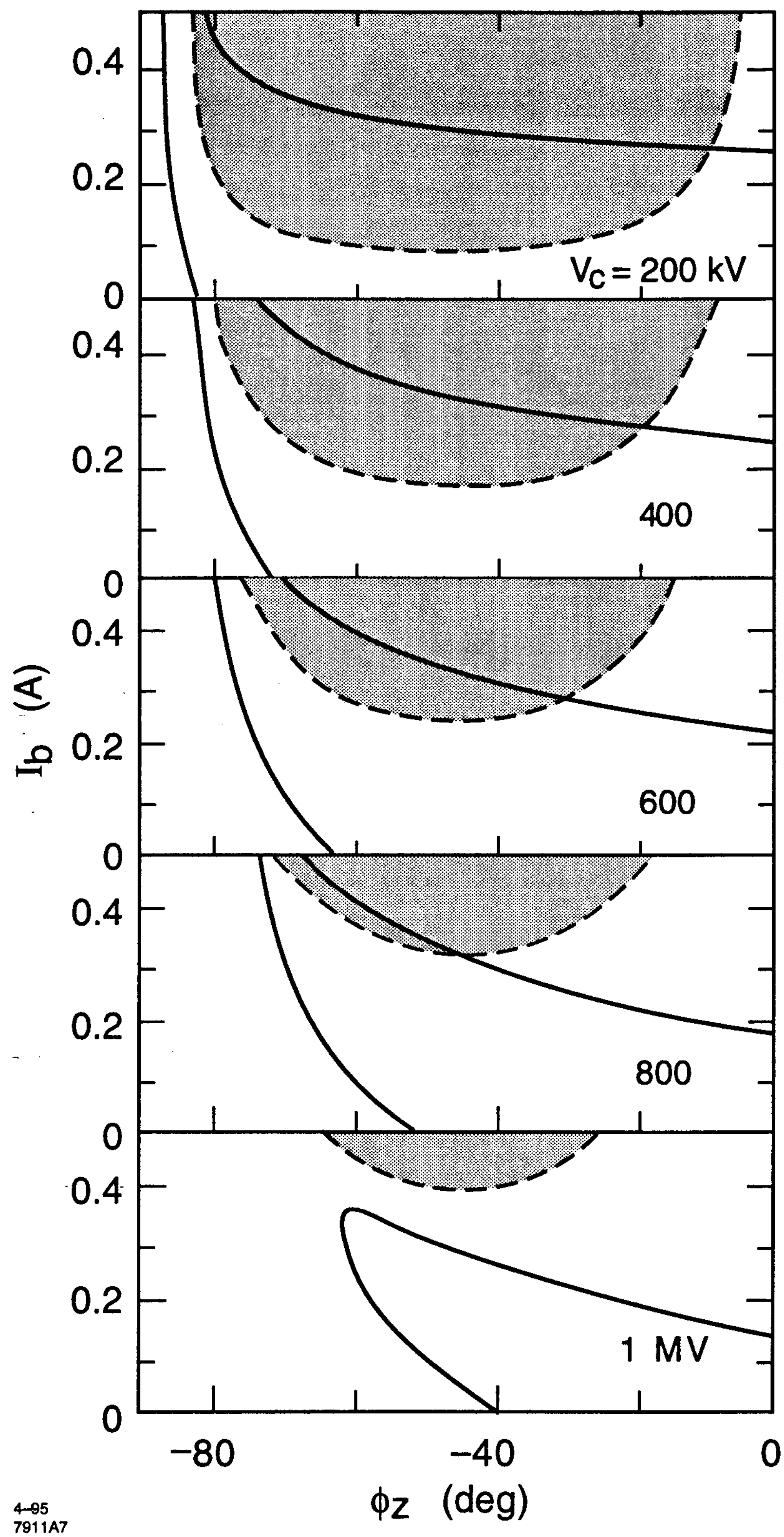

Fig. 6

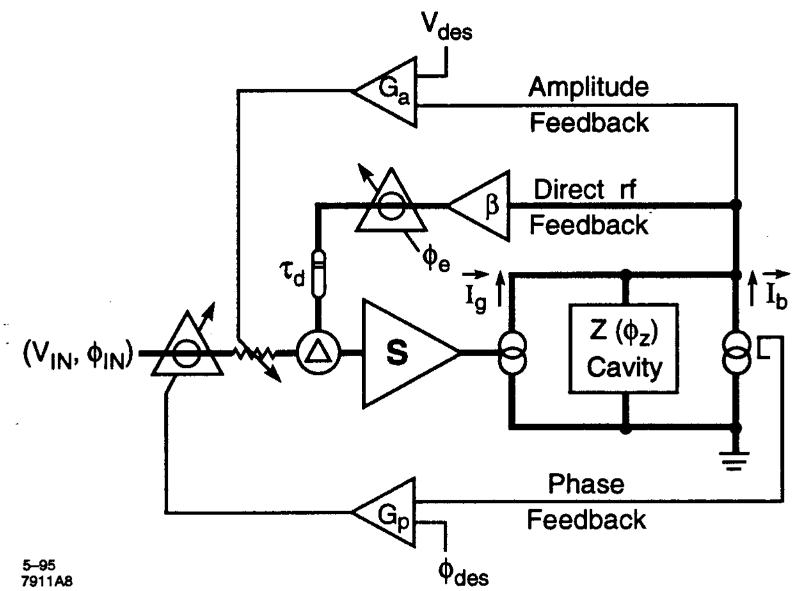

V_{des}
G_a
Amplitude
Feedback
Direct rf
Feedback
β
ϕ_e
τ_d
$\vec{I}_g$
$\vec{I}_b$
(V_{IN}, ϕ_{IN})
S
$Z(\phi_z)$
Cavity
Phase
Feedback
G_p
ϕ_{des}
5–95
7911A8

Fig. 7

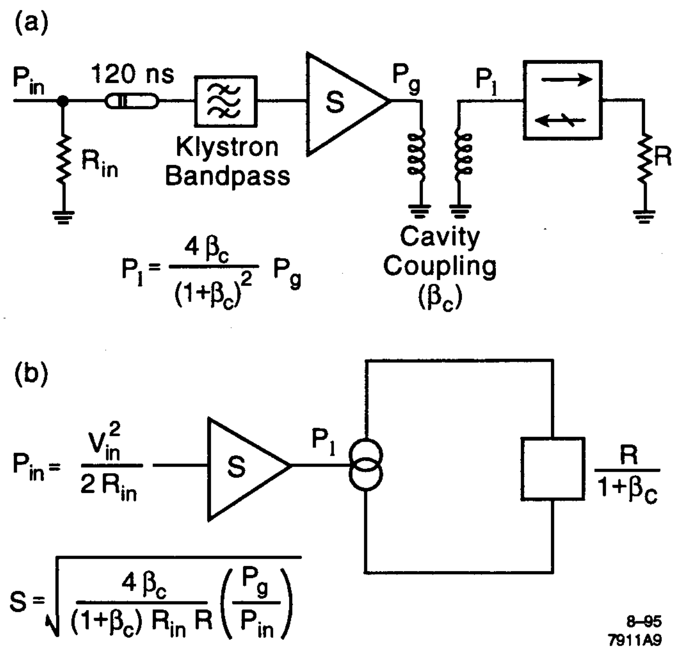
(a)
P_{in}
120 ns
R_{in}
Klystron
Bandpass
S
P_g
P_l
R
Cavity
Coupling
(β_c)
$P_l = \frac{4\beta_c}{(1+\beta_c)^2} P_g$
(b)
$P_{in} = \frac{V_{in}^2}{2R_{in}}$
S
P_l
$\frac{R}{1+\beta_c}$
$S = \sqrt{\frac{4\beta_c}{(1+\beta_c) R_{in} R}\left(\frac{P_g}{P_{in}}\right)}$
8-95
7911A9

Fig. 8

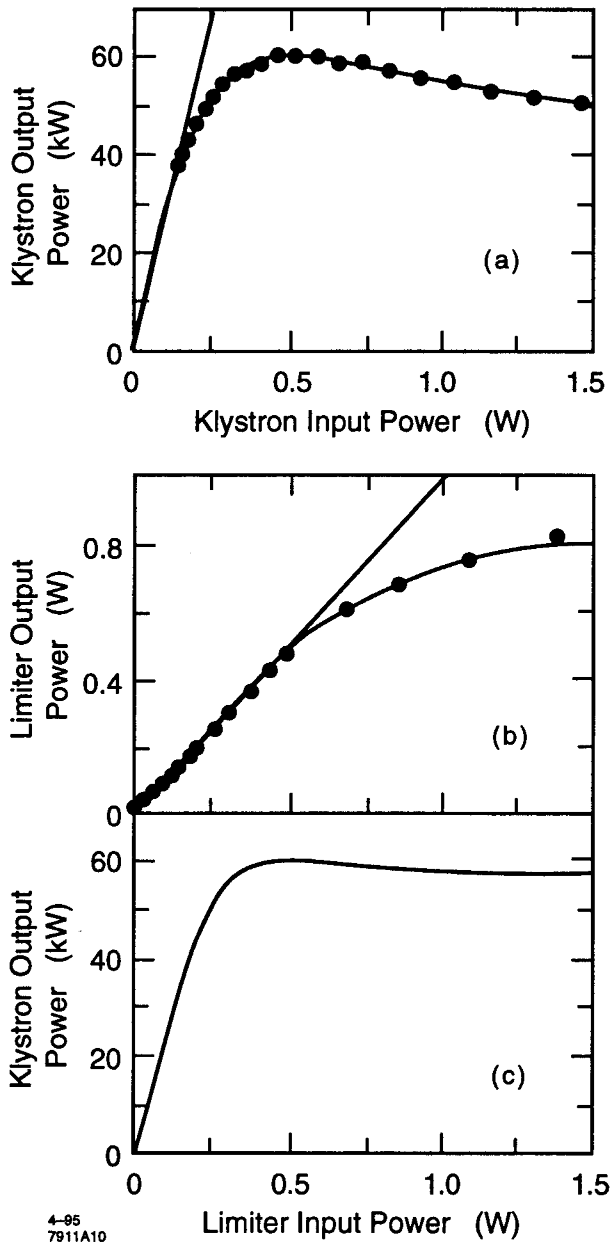
Klystron Output Power (kW)
60
40
20
0
(a)
0
0.5
1.0
1.5
Klystron Input Power (W)
Limiter Output Power (W)
0.8
0.4
0
(b)
Klystron Output Power (kW)
60
40
20
0
(c)
0
0.5
1.0
1.5
Limiter Input Power (W)
4–95
7911A10

Fig. 9

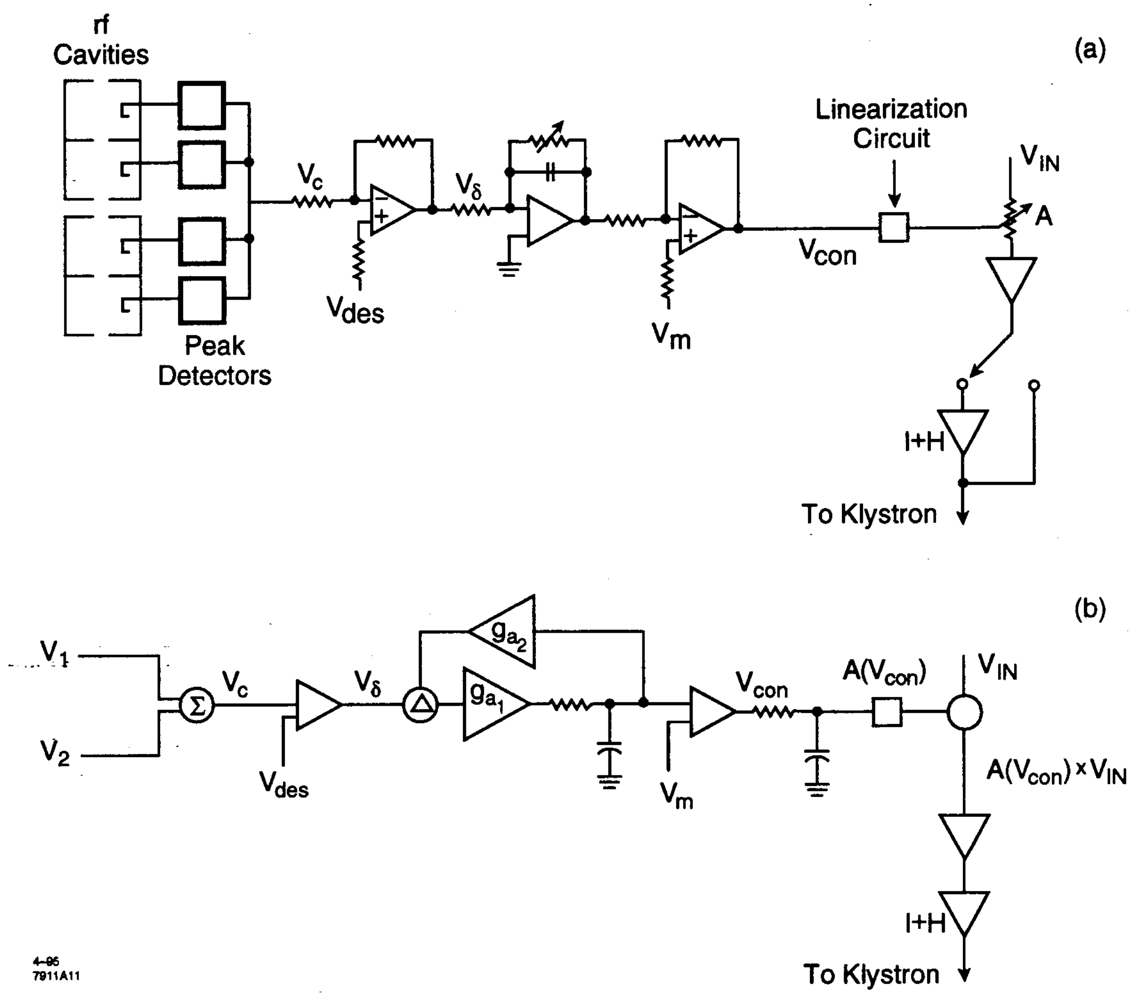
rf
Cavities
(a)
Peak
Detectors
V_c
V_δ
V_{des}
V_m
Linearization
Circuit
V_{con}
V_{IN}
A
I+H
To Klystron
(b)
V_1
V_2
V_c
V_δ
V_{des}
g_{a_2}
g_{a_1}
V_m
V_{con}
$A(V_{con})$
V_{IN}
$A(V_{con}) \times V_{IN}$
I+H
To Klystron
4-95
7911A11

Fig. 10

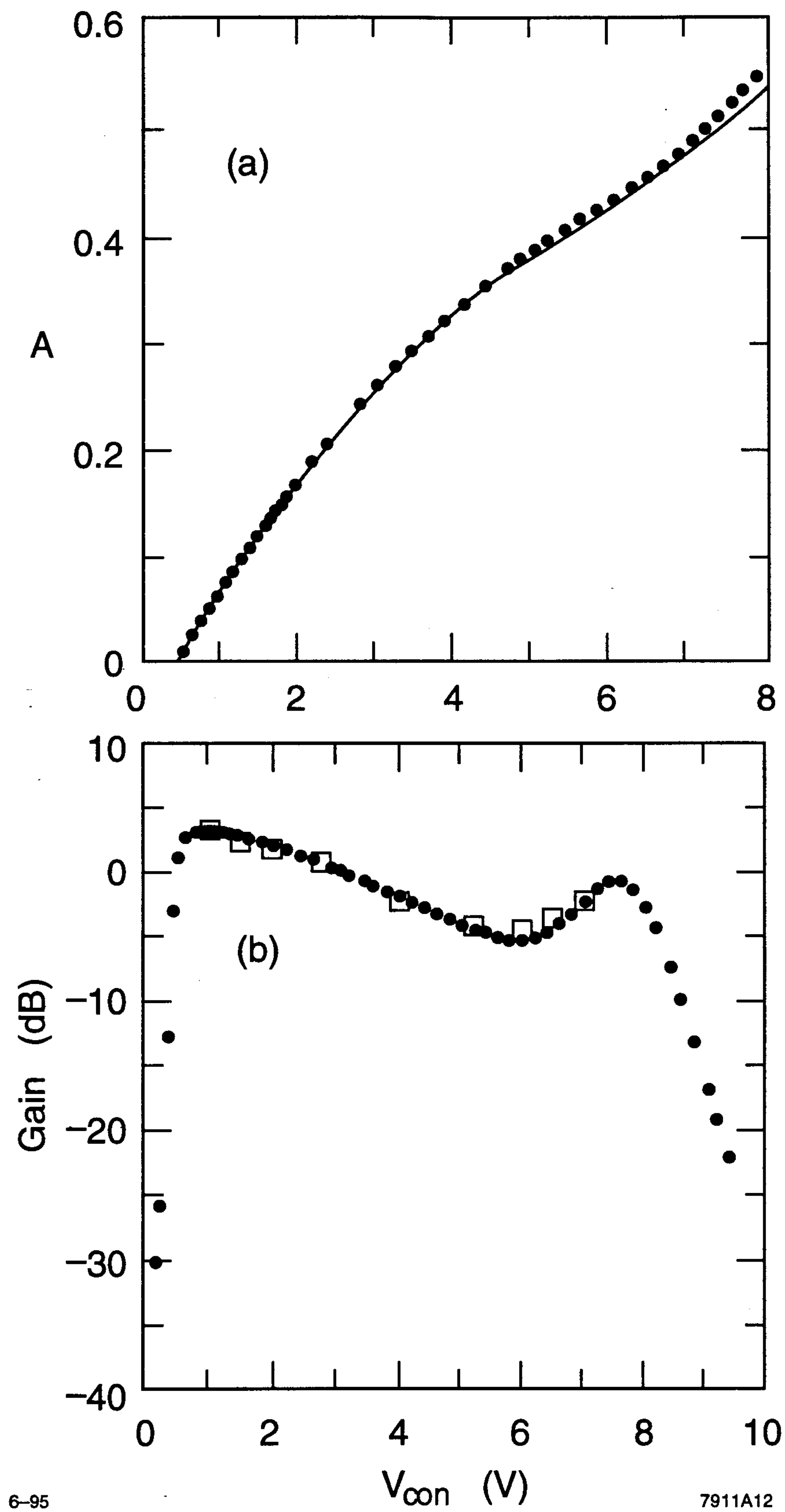
0.6
(a)
0.4
A
0.2
0
0
2
4
6
8
10
0
(b)
−10
Gain (dB)
−20
−30
−40
0
2
4
6
8
10
Vcon (V)
6–95
7911A12

Fig. 11

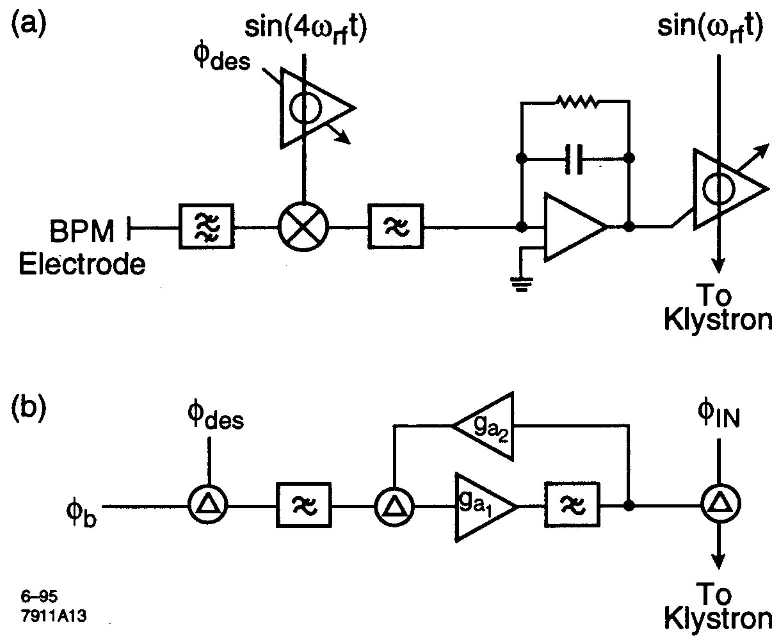
(a)
sin(4ωrft)
φdes
sin(ωrft)
BPM
Electrode
To
Klystron
(b)
φdes
ga2
φIN
φb
ga1
To
Klystron
6–95
7911A13

Fig. 12

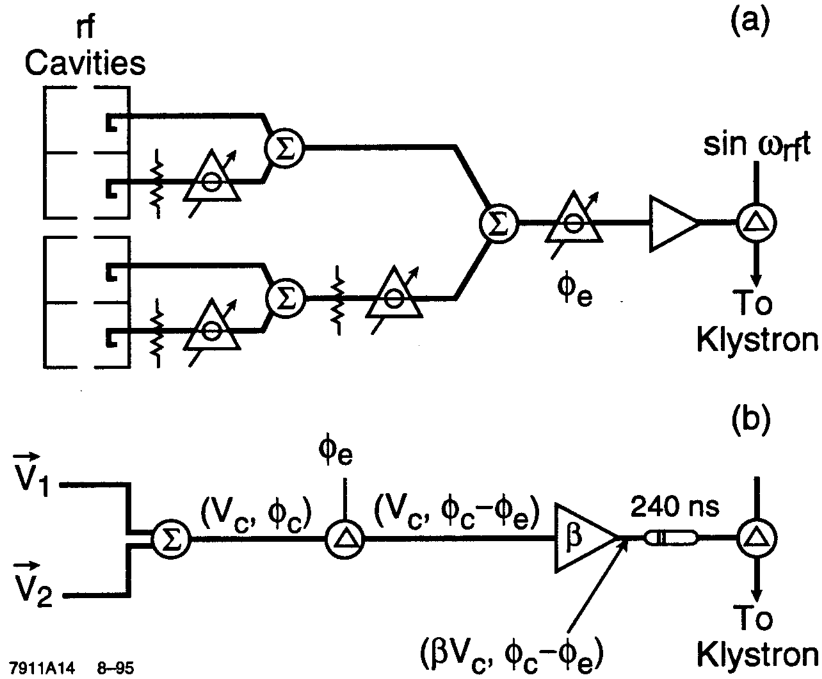

rf
Cavities
(a)
sin ωrft
φe
To
Klystron
(b)
φe
V1
V2
(Vc, φc)
(Vc, φc−φe)
β
240 ns
To
Klystron
(βVc, φc−φe)
7911A14 8–95

Fig. 13

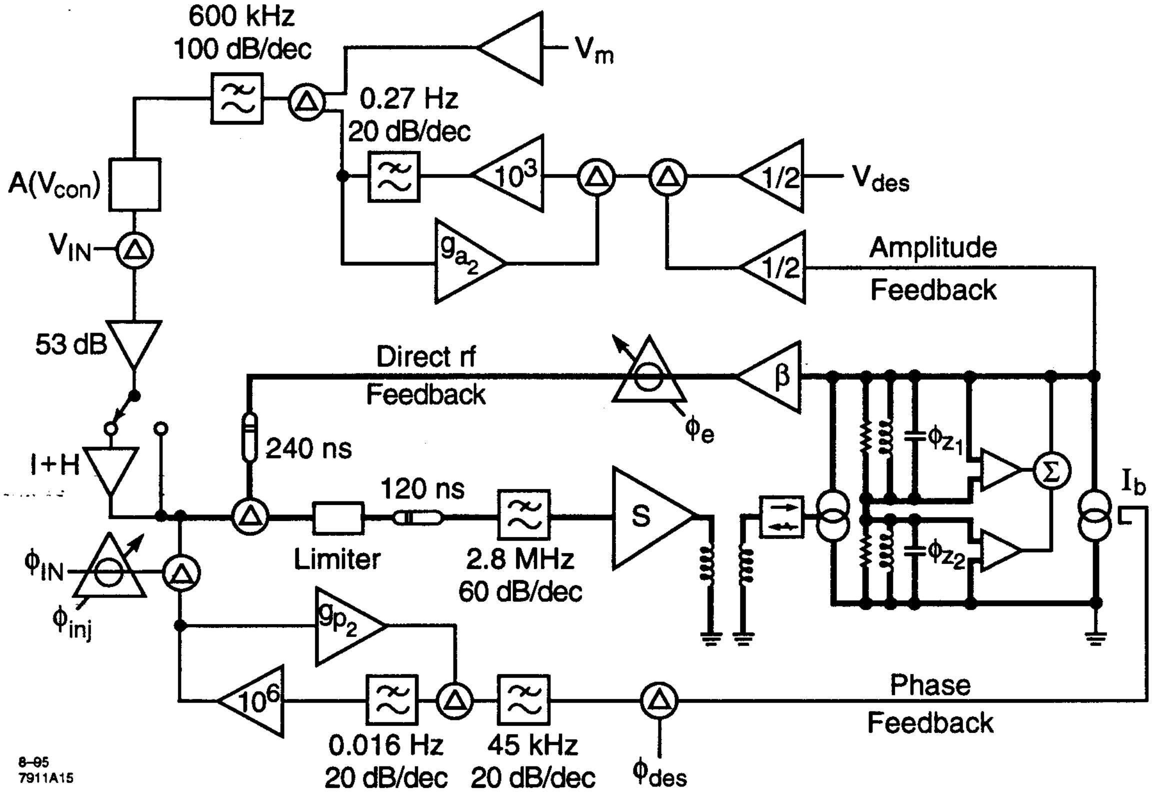

600 kHz
100 dB/dec
Vm
0.27 Hz
20 dB/dec
A(Vcon)
10^3
1/2
Vdes
VIN
ga2
1/2
Amplitude
Feedback
53 dB
Direct rf
Feedback
β
240 ns
φe
I+H
120 ns
φz1
Σ
Ib
S
φIN
Limiter
2.8 MHz
60 dB/dec
φz2
φinj
gp2
Phase
Feedback
10^6
0.016 Hz
20 dB/dec
45 kHz
20 dB/dec
φdes
8-95
7911A15

Fig. 14

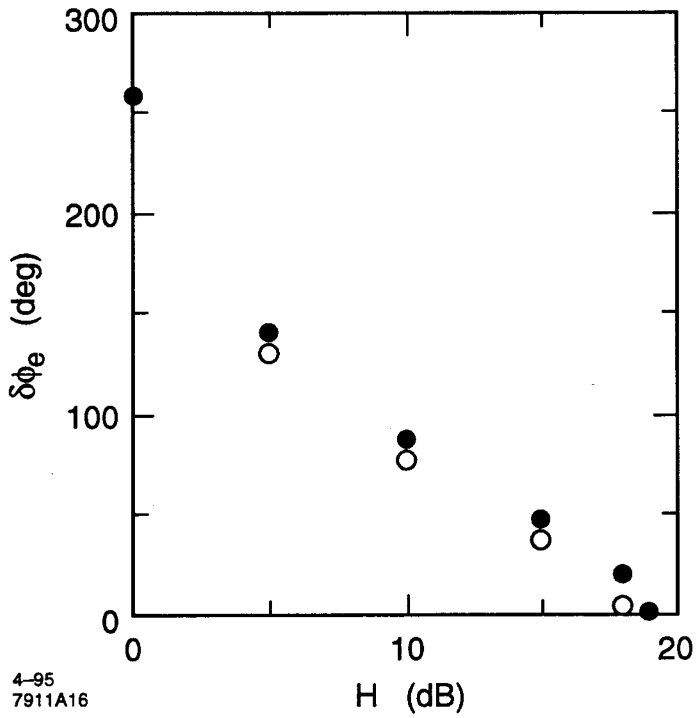

Fig. 15

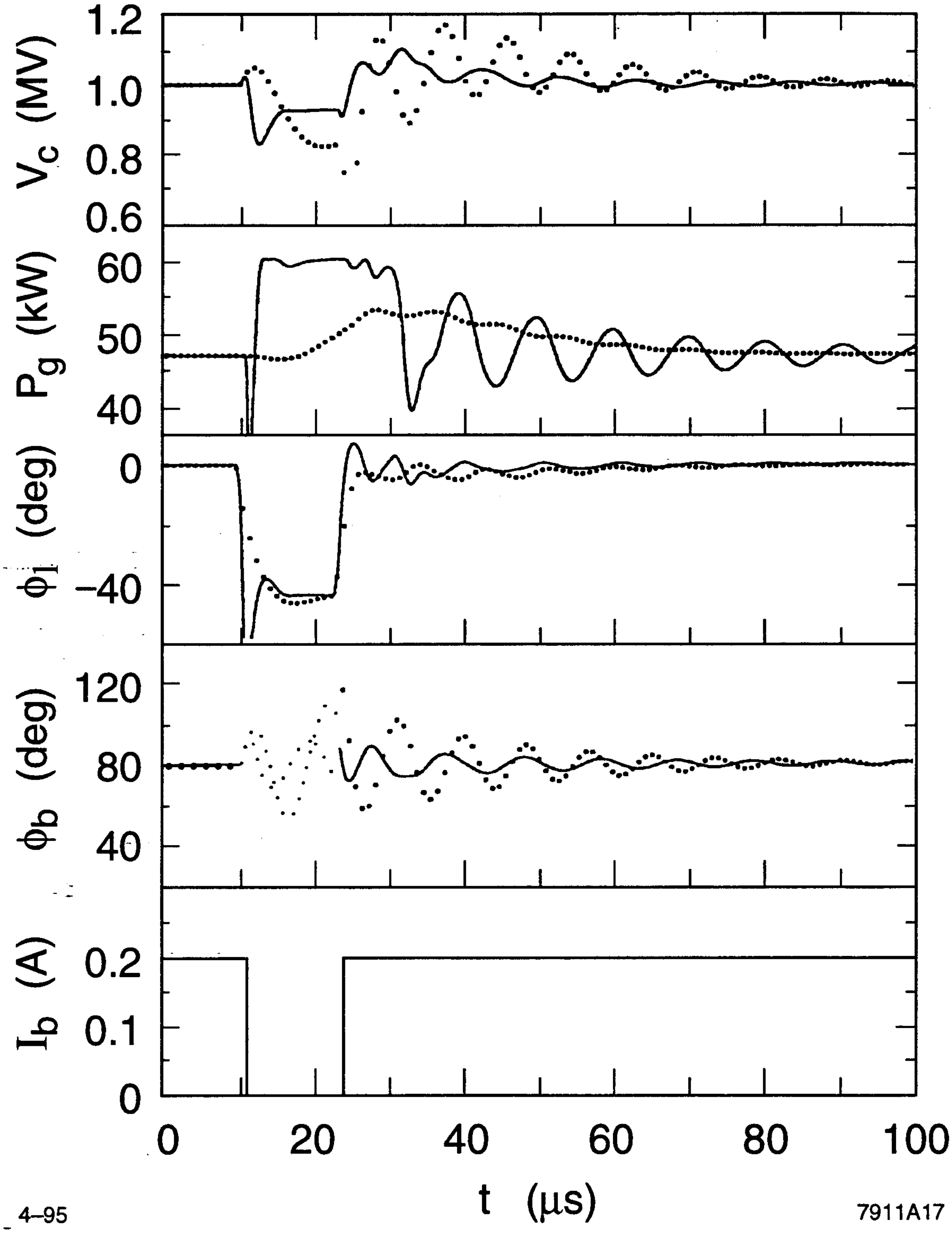

1.2
1.0
0.8
0.6
V_c (MV)
60
50
40
P_g (kW)
0
−40
ϕ_i (deg)
120
80
40
ϕ_b (deg)
0.2
0.1
0
I_b (A)
0
20
40
60
80
100
t (μs)
4–95
7911A17

Fig. 16

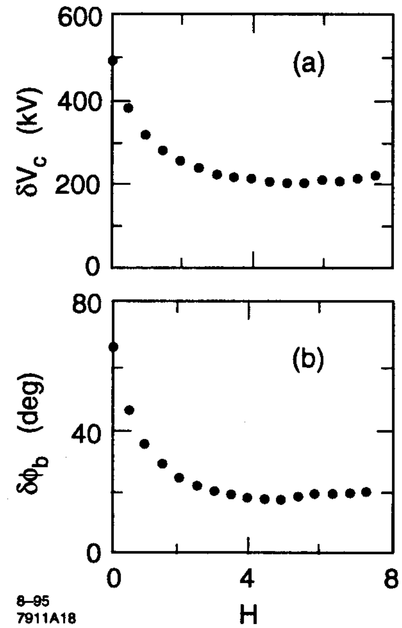

Fig. 17

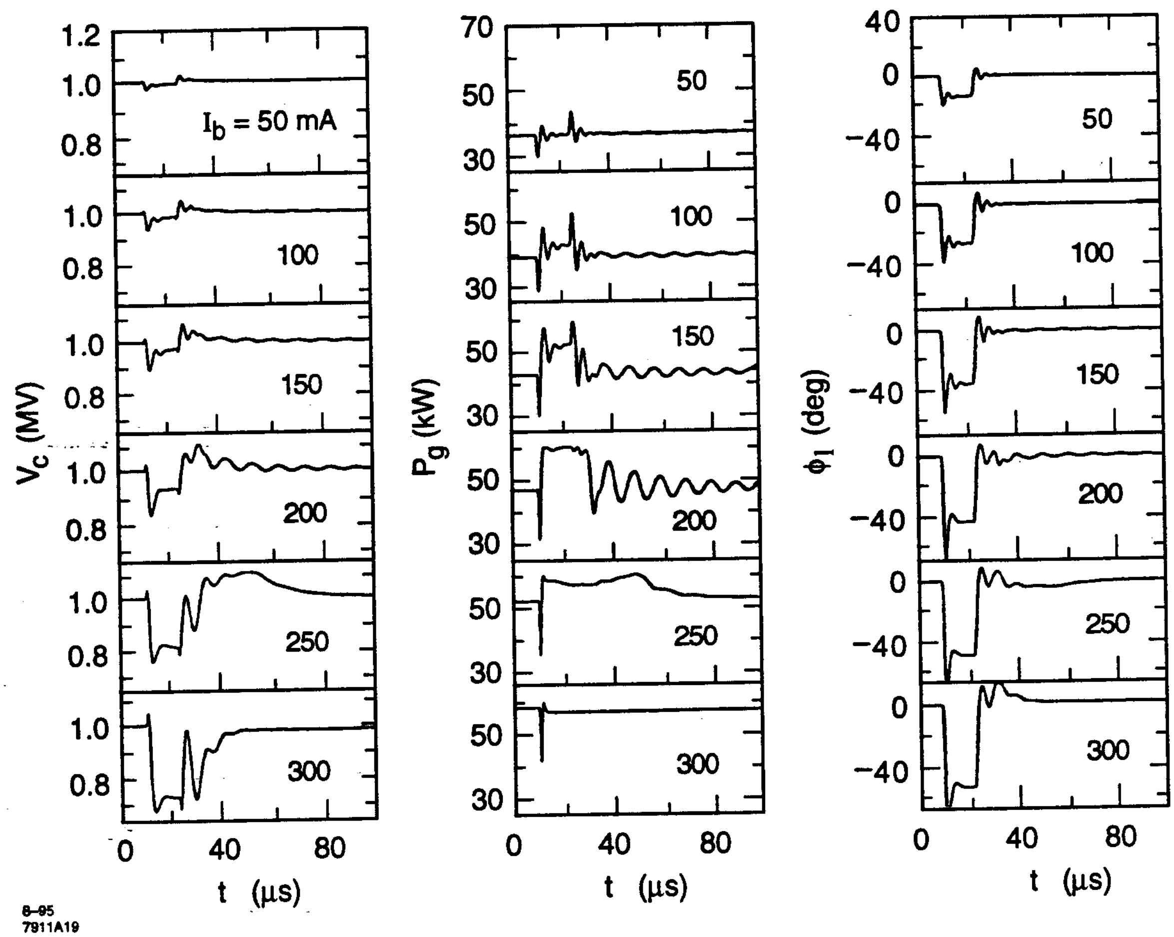

1.2
1.0
0.8
I_b = 50 mA
100
150
200
250
300
V_c (MV)
0
40
80
t (µs)
70
50
30
P_g (kW)
40
0
−40
ϕ_1 (deg)
8-95
7911A19

Fig. 18

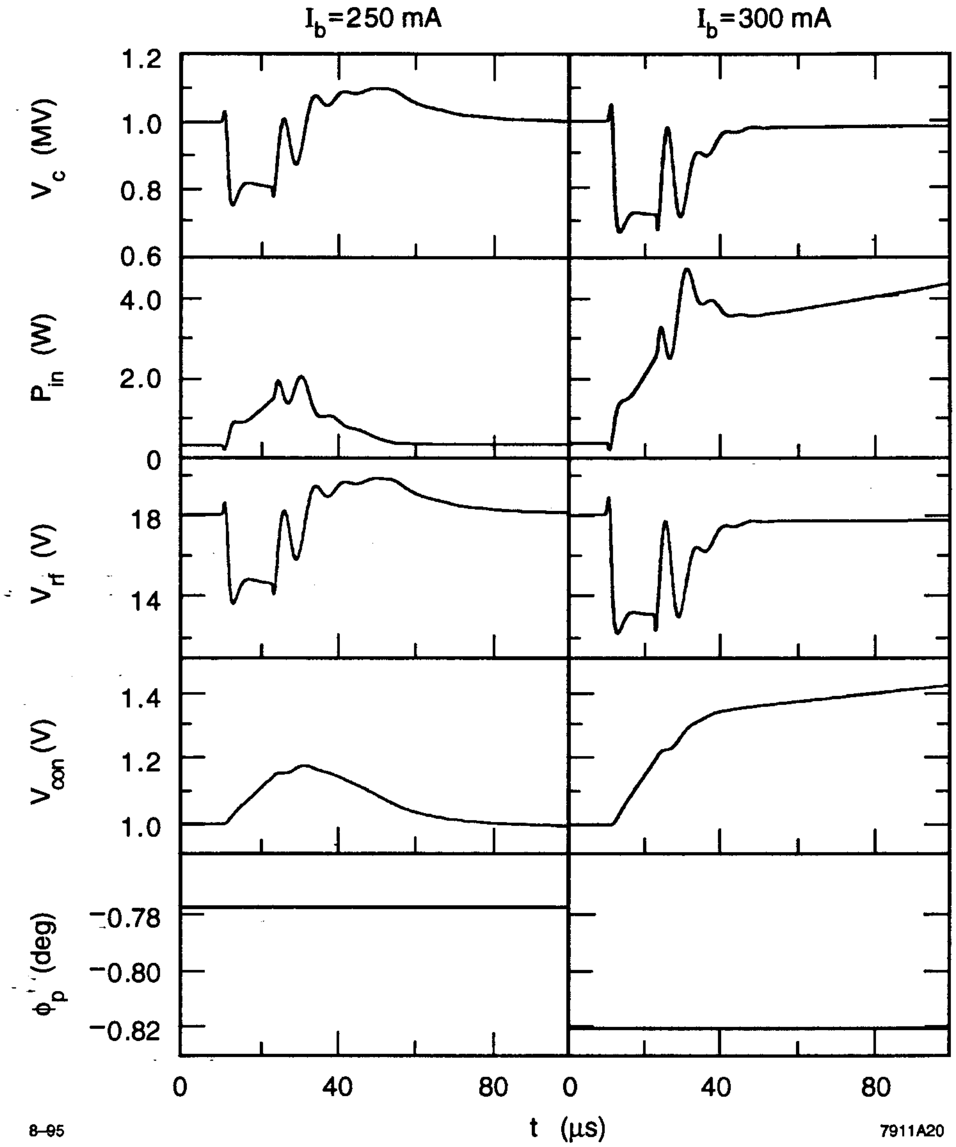

I_b=250 mA
I_b=300 mA
V_c (MV)
1.2
1.0
0.8
0.6
P_in (W)
4.0
2.0
0
V_rf (V)
18
14
V_con (V)
1.4
1.2
1.0
φ_p (deg)
−0.78
−0.80
−0.82
0
40
80
0
40
80
t (μs)
8–95
7911A20

Fig. 19

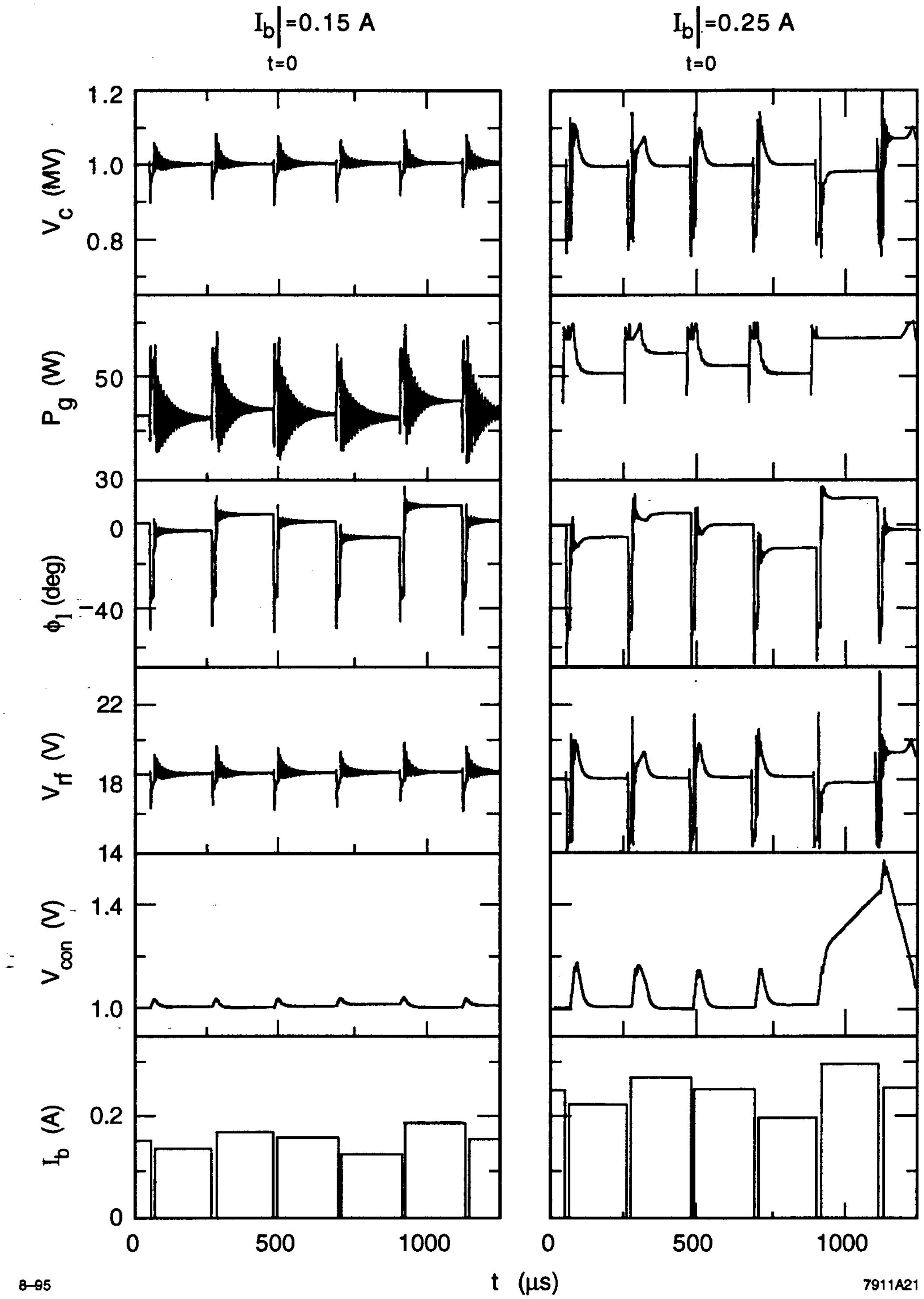

$I_b|$=0.15 A
t=0
$I_b|$=0.25 A
t=0
1.2
1.0
0.8
V_c (MV)
50
30
P_g (W)
0
−40
ϕ_l (deg)
22
18
14
V_{rf} (V)
1.4
1.0
V_{con} (V)
0.2
0
I_b (A)
0
500
1000
t (μs)
8–95
7911A21

Fig. 20

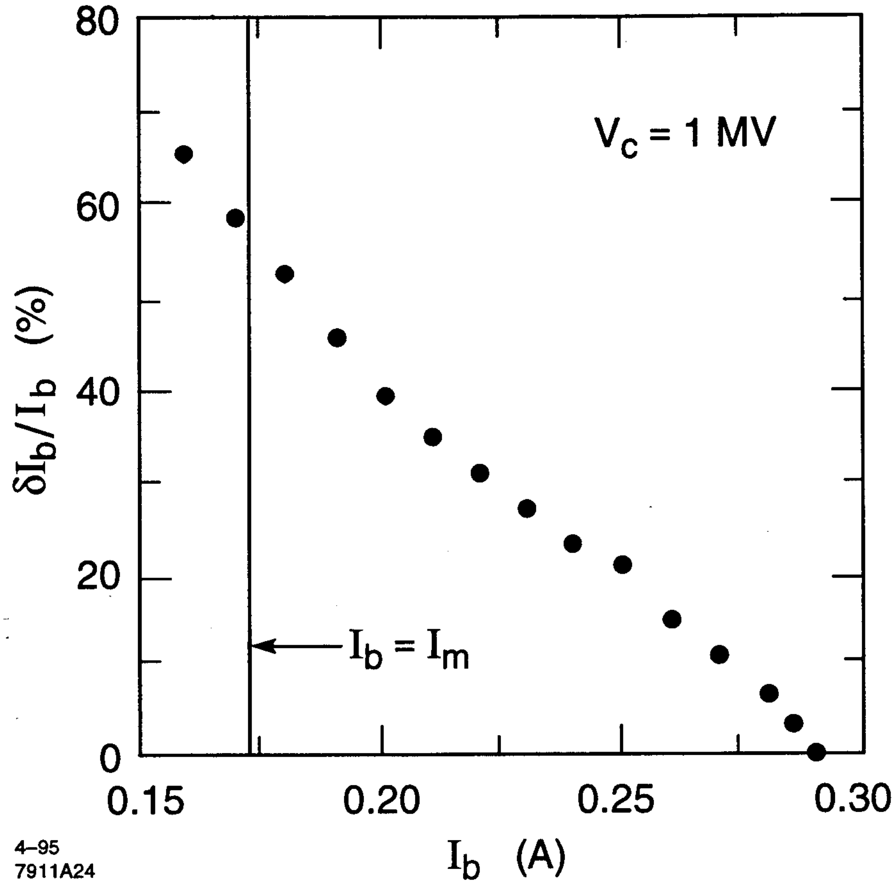
80
60
40
20
0
0.15
0.20
0.25
0.30
V_c = 1 MV
$I_b = I_m$
$\delta I_b/I_b$ (%)
I_b (A)
4–95
7911A24

Fig. 21

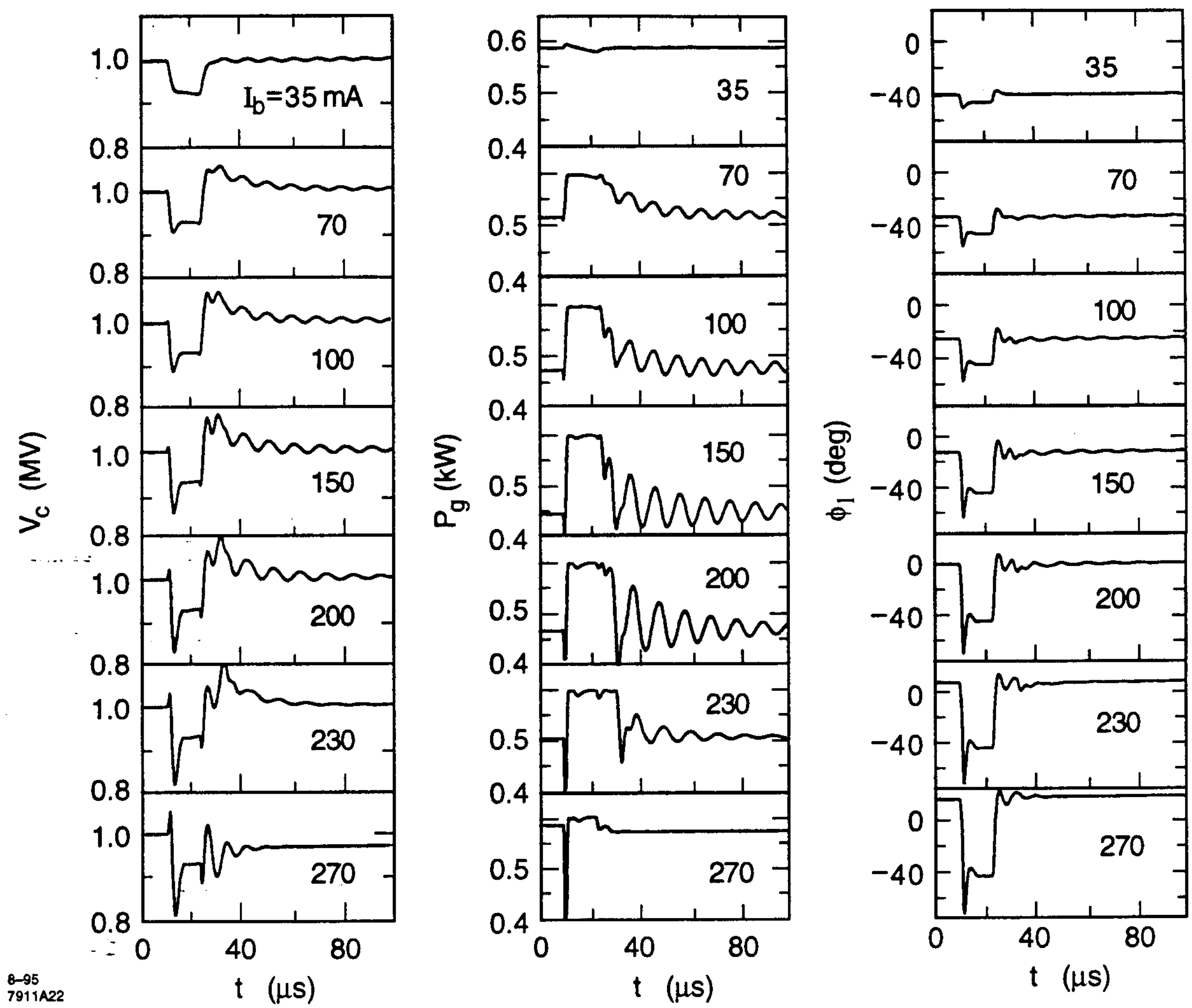
I_b=35 mA
70
100
150
200
230
270
35
V_c (MV)
P_g (kW)
ϕ_1 (deg)
t (μs)
8–95
7911A22

Fig. 22

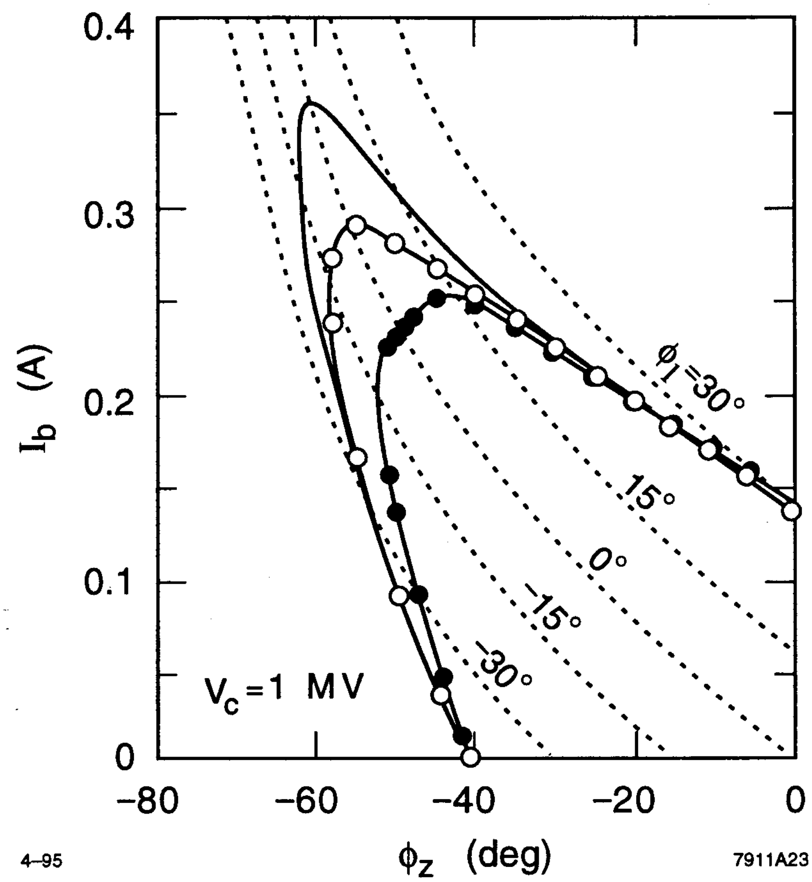

0.4
0.3
0.2
0.1
0
I_b (A)
−80
−60
−40
−20
0
ϕ_z (deg)
ϕ_l =30°
15°
0°
−15°
−30°
V_c =1 MV
4–95
7911A23

Fig. 23

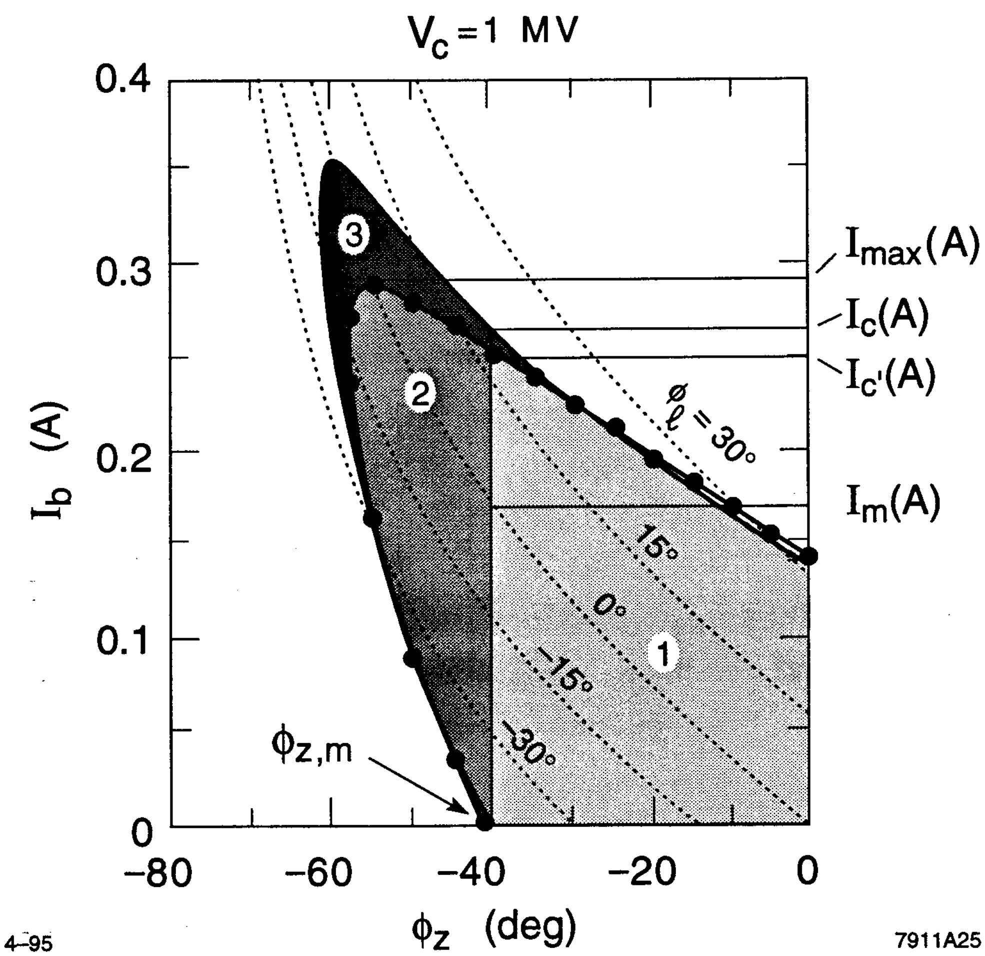

Vc =1 MV
0.4
0.3
0.2
0.1
0
−80
−60
−40
−20
0
Ib (A)
ϕz (deg)
Imax(A)
Ic(A)
Ic'(A)
Im(A)
φℓ = 30°
15°
0°
−15°
−30°
1
2
3
ϕz,m
4-95
7911A25

Fig. 24

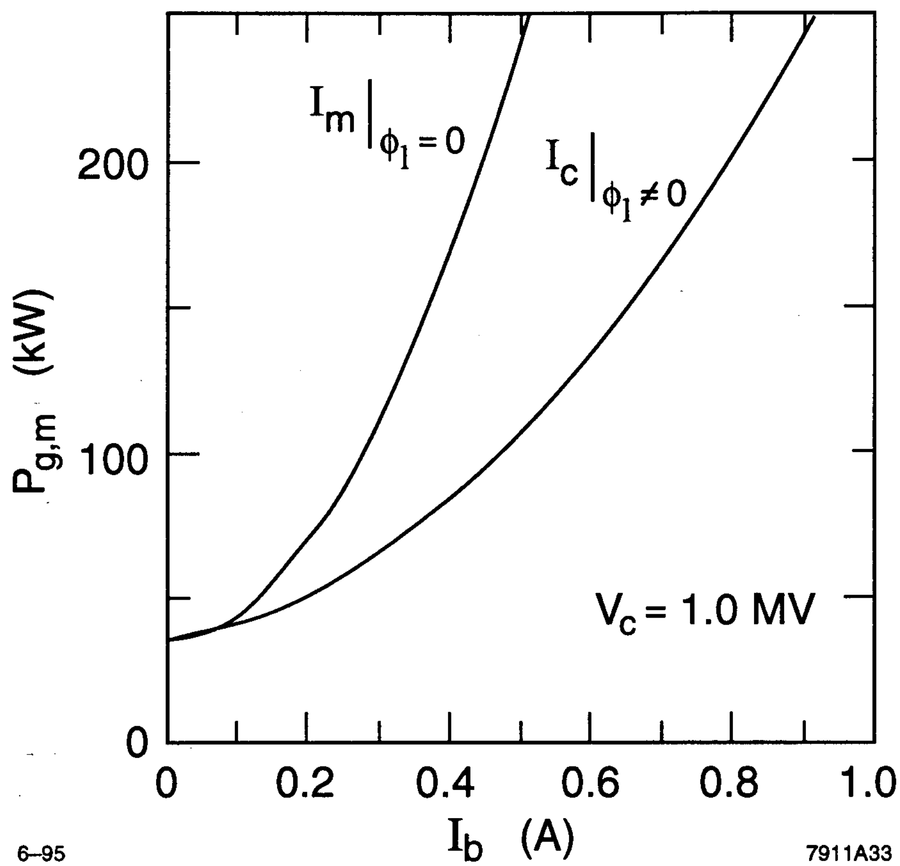

200
100
0
0
0.2
0.4
0.6
0.8
1.0
$P_{g,m}$ (kW)
I_b (A)
$I_m|_{\phi_1=0}$
$I_c|_{\phi_1\neq 0}$
$V_c = 1.0$ MV
6–95
7911A33

Fig. 25

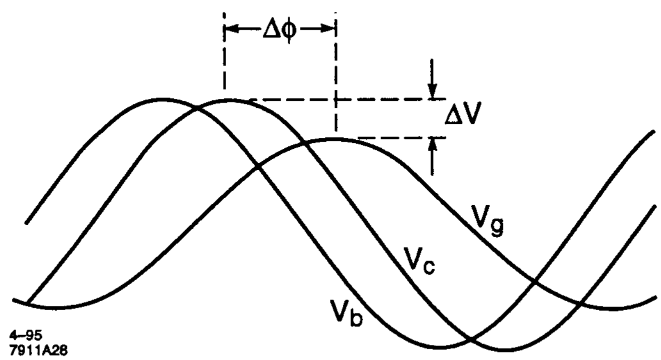

Fig. 26

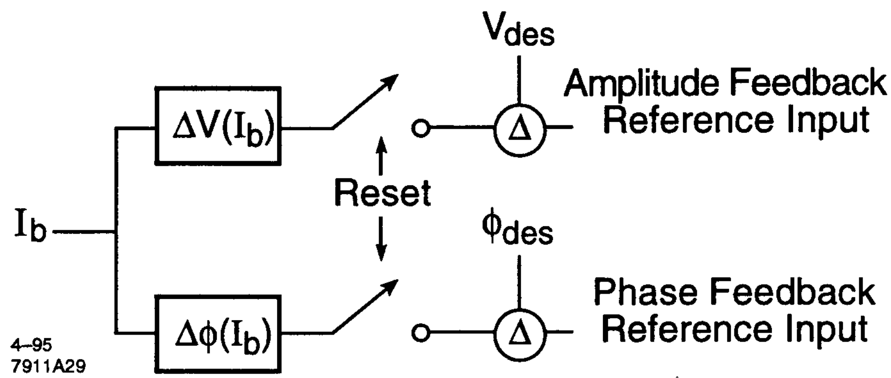
V_{des}
Amplitude Feedback
Reference Input
$\Delta V(I_b)$
Reset
I_b
ϕ_{des}
Phase Feedback
Reference Input
$\Delta\phi(I_b)$
Δ
Δ
4–95
7911A29

Fig. 27

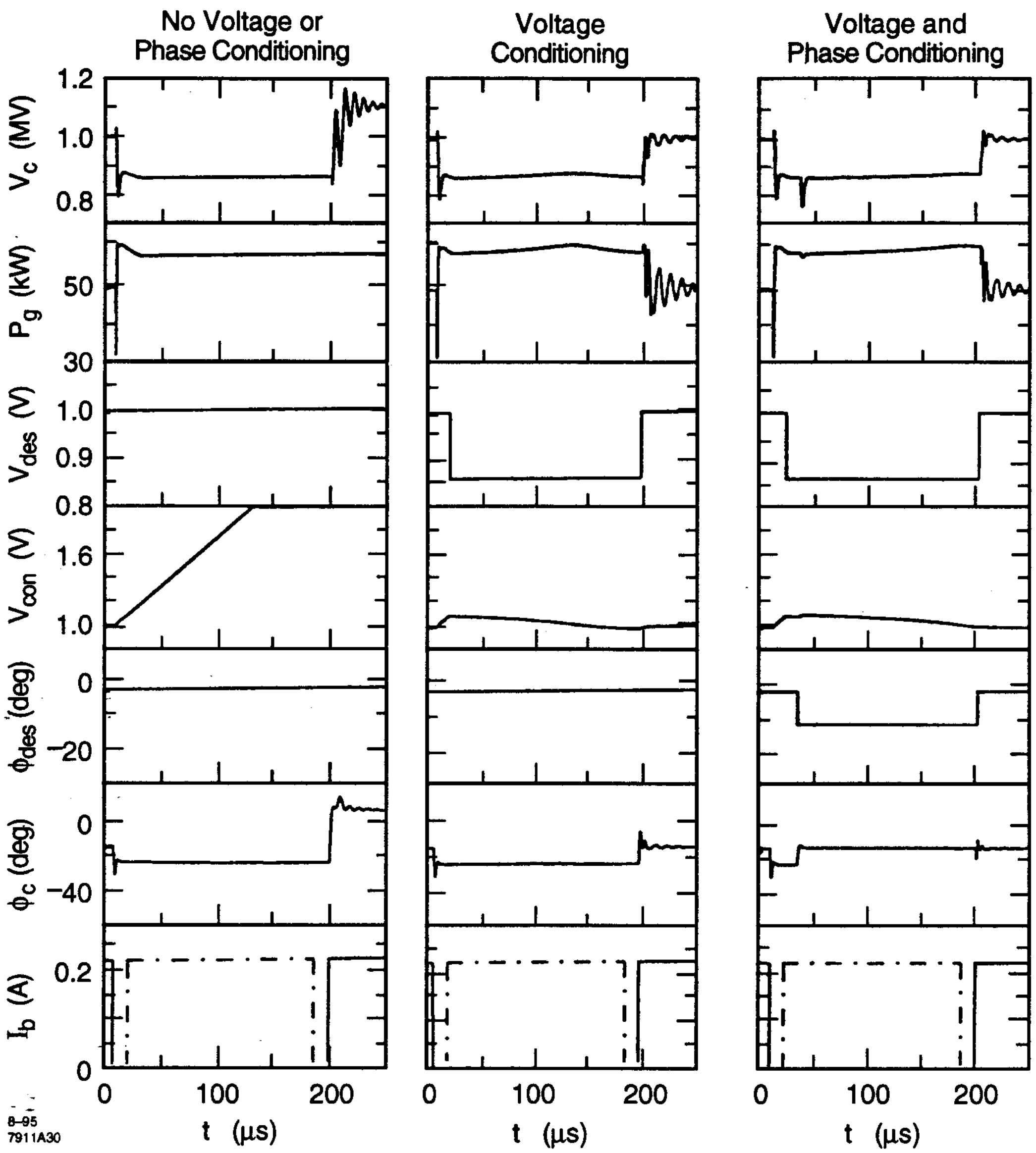

No Voltage or Phase Conditioning
Voltage Conditioning
Voltage and Phase Conditioning
V_c (MV)
1.2
1.0
0.8
P_g (kW)
50
30
V_{des} (V)
1.0
0.9
0.8
V_{con} (V)
1.6
1.0
ϕ_{des} (deg)
0
−20
ϕ_c (deg)
0
−40
I_b (A)
0.2
0
0
100
200
t (μs)
8–95
7911A30

Fig. 28

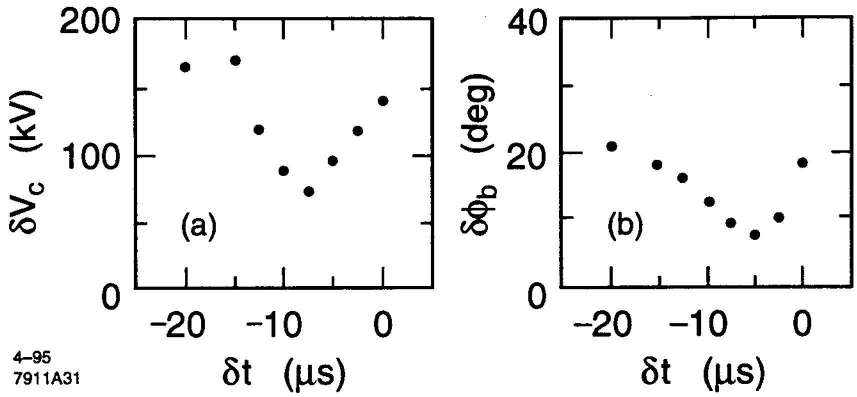
200
100
0
δVc (kV)
(a)
−20
−10
0
δt (μs)
40
20
0
δϕb (deg)
(b)
−20
−10
0
δt (μs)
4–95
7911A31

Fig. 29

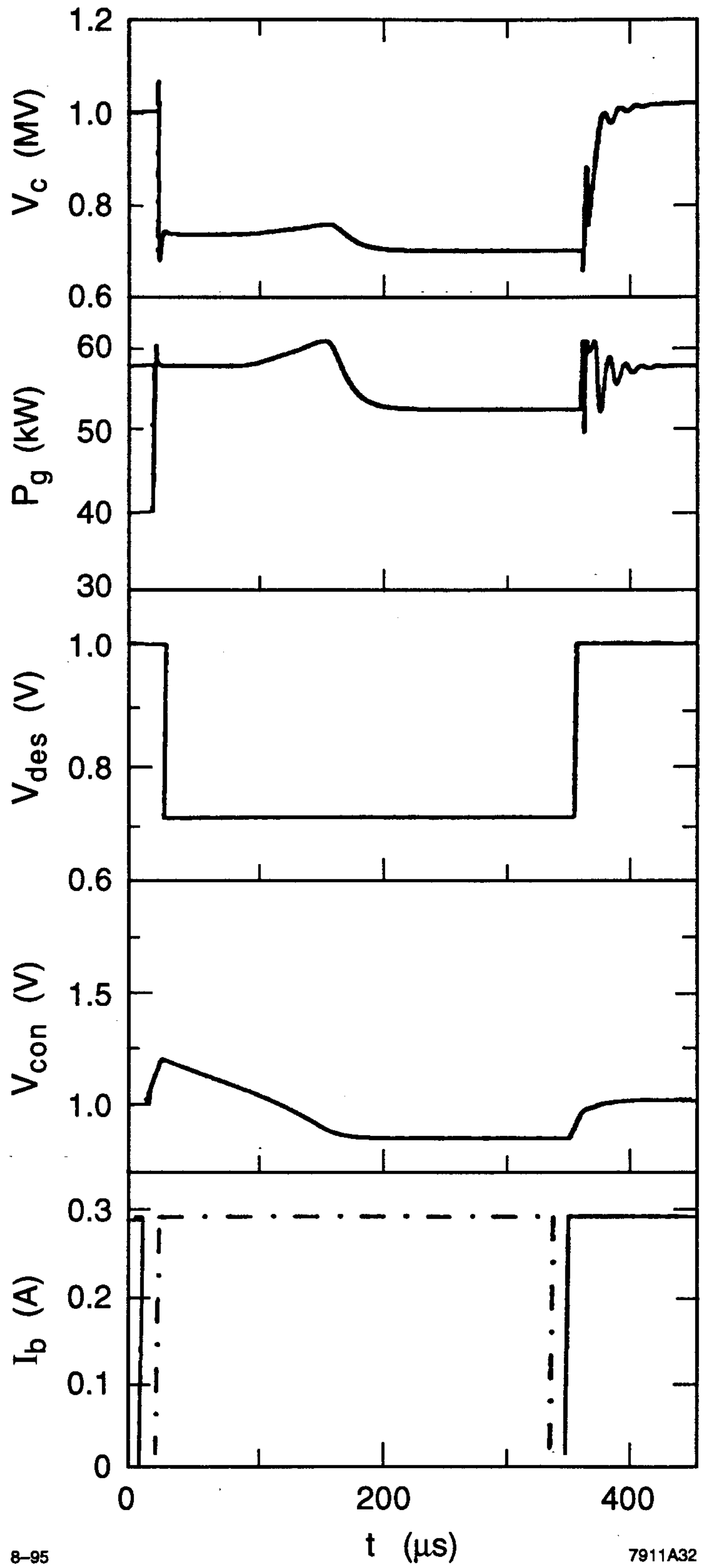

1.2
1.0
0.8
0.6
V_c (MV)
60
50
40
30
P_g (kW)
1.0
0.8
0.6
V_{des} (V)
1.5
1.0
V_{con} (V)
0.3
0.2
0.1
0
I_b (A)
0
200
400
t (μs)
8–95
7911A32

Fig. 30